Molecular Cell

CellPress

Article

TRiC/CCT chaperonin governs RNA polymerase II activity in the nucleus to support RNA homeostasis

Zlata Gvozdenov,[1,2] Anusmita Biswas,[1,4] Audrey Yi Tyan Peng,[1,4] Zeno Barcutean,[1] Daniel Gestaut,[3] Judith Frydman,[3] Kevin Struhl,[2] and Brian C. Freeman[1,5,*]

[1]Department of Cell and Developmental Biology, School of Molecular and Cellular Biology, University of Illinois-Urbana-Champaign, Urbana, IL 61801, USA

[2]Department of Biological Chemistry and Molecular Pharmacology, Harvard Medical School, Boston, MA 94305, USA

[3]Department of Biology, Stanford University, Stanford, CA 02115, USA

[4]These authors contributed equally

[5]Lead contact

*Correspondence: bfree@illinois.edu

https://doi.org/10.1016/j.molcel.2026.08.015

SUMMARY

Eukaryotic tailless complex polypeptide 1 ring complex/Chaperonin containing tailless complex polypeptide 1 (TRiC/CCT) chaperonin is typically considered a cytosolic machine mediating polypeptide folding and assembly of protein complexes. Here, we investigated the nuclear role of TRiC/CCT. Use of a TRiC/CCT temperature-sensitive allele revealed increased production of nascent RNA leading to the accumulation of noncoding transcripts. TRiC/CCT was associated with RNA polymerase II (RNAPII) *in vitro* and *in vivo*, including when bound to DNA. Heat treatment of the TRiC/CCT *ts* chaperonin stabilized the RNAPII complex association and binding to the actin and tubulin substrates. Expression of the Huntingtin protein Htt correlated with lowered RNA production and a decreased association between the RNAPII and TRiC/CCT complexes. Together, our presented data support a model where TRiC/CCT regulates the global activity of RNAPII in reaction to the status of proteostasis. Overall, our work reveals an avenue by which TRiC/CCT contributes to homeostasis by regulating the activity of nuclear RNAPII.

INTRODUCTION

The molecular chaperone tailless complex polypeptide 1 ring complex (TRiC) or Chaperonin containing tailless complex polypeptide 1 (CCT) is an essential eukaryotic chaperonin distantly related to prokaryotic GroEL.[1] All chaperonins are multi-subunit oligomers forming 2 stacked rings with TRiC consisting of 8 paralogous subunits (Cct1–Cct8) in each ring with an evolutionarily conserved arrangement.[1] Classically, the chaperonins are considered assembly factors of biological complexes. GroEL was originally identified as an essential host factor for the replication of bacteriophages where it assembles phage capsids (Gro, phage growth; E, growth defect overcome by mutation in phage head protein; L, large subunit).[2,3] Since these founding studies, it has been shown that GroEL also aides in nascent polypeptide folding, prompts the disassembly of protein structures, and is induced to facilitate stress resistance.[4–8] While TRiC also mediates *de novo* protein folding and complex assembly, it is not stress inducible.[9,10] In general, our understanding of eukaryotic chaperonins remains limited.

It is well established that cytoplasmic TRiC promotes the co- and post-translational maturation of ~10% of new polypeptides including many essential and topologically intricate factors including actin, tubulin, and beta-propeller factors such as F-box and G-beta proteins.[6,7,11–14] Similar to GroEL, a common TRiC/CCT activity is the assembly of protein complexes. For instance, TRiC is needed for the formation of VHL-Elongin BC tumor suppressor structure, the Gβγ dimer, the Bardet-Biedl syndrome protein structure, and the basal transcription factor complex TFIID.[15–18] However, TRiC does not only contribute to polypeptide folding but can have regulatory functions, as is the case when TRiC interacts with gelsolin where the chaperonin regulates the activity of this actin capping/severing factor.[19,20] Furthermore, TRiC does not fold Orai1 but rather modulates the intracellular trafficking of the native Orai1 membrane protein, which influences calcium signaling kinetics.[21] Perhaps, it is the multiple contributions of TRiC to various eukaryotic cellular pathways that makes it an essential eukaryotic factor.[22]

Potentially complicating the full understanding of TRiC function is the division of eukaryotic cells into distinct compartments. While it is clear that prokaryotic-origin mitochondria contain the chaperonin Hsp60, which is more similar to GroEL, whether TRiC works just in the cytosol or if it has a nuclear role is not understood. TRiC was originally defined as a cytoplasmic machine.[23] Yet, several

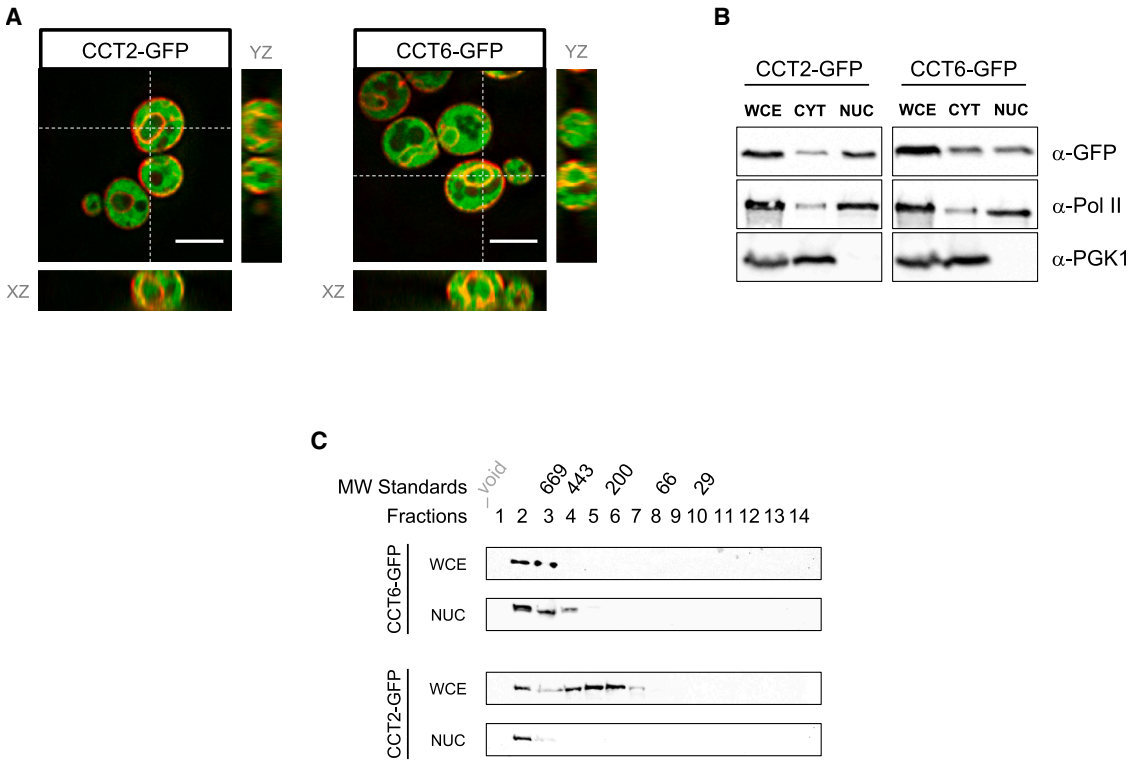

Figure 1. TRiC has a presence in both the cytoplasm and nucleoplasm

(A) The cellular localization of TRiC was visualized using yeast expressing GFP fusions of the Cct2 or Cct6 subunits,[40] as marked. Confocal images were acquired using an Airyscan 2 LSM 900.

(B) Yeast cells were biochemically separated into cytosolic and nucleosolic fractions. Markers for the nuclear (RNA polymerase α-Pol II) and cytosol (phosphoglycerate kinase 1 α-PGK1) compartments were followed by immunoblot analysis as well as the position of GFP-Cct2 or GFP-Cct6 (α-GFP), as marked.

(C) To check if GFP-Cct2 and GFP-Cct6 assembled into the chaperonin structure in the nucleoplasm, whole cell and nuclear extracts were resolved by size exclusion chromatography and the position of GFP-Cct2 or GFP-Cct6 were visualized by immunoblot analysis. The relative positions of native protein size standards (units are kDa) are shown above the fractions.

studies have reported TRiC subunits in the nucleus and/or associated with nuclear factors including the detection of TRiC subunits in the nucleus.[24–26] TRiC-P5 was reported in a large complex associated with the nuclear matrix of human lymphocytes and leukocytes; human TCP1 isoforms localize to the nuclear matrix during apoptotic chromatin condensation, and mouse TRiC interacts with heterochromatin during spermatogenesis.[27–30] High-throughput mass spectrometry studies and selective ribosome profiling analyses have physically connected TRiC to several nuclear factors including components of histone deacetylases (Set3C, Rpd3S, and Rpd3L), histone acetylase (SAGA), chromatin remodelers (SWR-C and SWI/SNF), methyltransferase (Set1C), basal transcription factor (TFIID), RNA metabolism (CCR4-NOT), and RNA polymerase II (RNAPII).[6,7,31–35] While the functional role of TRiC with each of these complexes is yet to be resolved, TRiC has been shown to fold subunits of the SMRT-HDAC3, TFIID, and telomerase complexes and to assemble these subunits into their final structures.[18,36] Whether TRiC interacts with these factors in the cytoplasm and/or nucleoplasm is not clear. Perhaps notably, the GroEL chaperonin is associated with bacterial RNA metabolism including RNA production and mRNA protection.[37–39] Here, we assessed the functional influence of TRiC on several nuclear pathways and show that TRiC localizes to the nucleus governing RNAPII activity to support nuclear RNA homeostasis.

RESULTS

TRiC has a nuclear presence

We began our chaperonin investigation by determining the cellular localization of TRiC in budding yeast cells. We exploited 2 TRiC subunits, Cct2 and Cct6, expressed as GFP fusions within a flexible surface loop of these subunits that does not interfere with chaperonin assembly and function.[40] We checked the localization of Cct2-GFP and Cct6-GFP by confocal fluorescent microscopy and biochemical fractionation. Both assays indicated a nuclear presence of TRiC (Figures 1A and 1B). To confirm that these represent the assembled chaperonin, we resolved the nuclear extract by size exclusion chromatography. We observed comparable patterns for Cct2-GFP and Cct6-GFP in nuclear or whole cell extracts with the fully assembled TRiC complex resolving into fraction 2 (Figure 1C). Hence, eukaryotic TRiC is present in the nucleus and is assembled into the ~1 MDa holo-chaperonin complex.

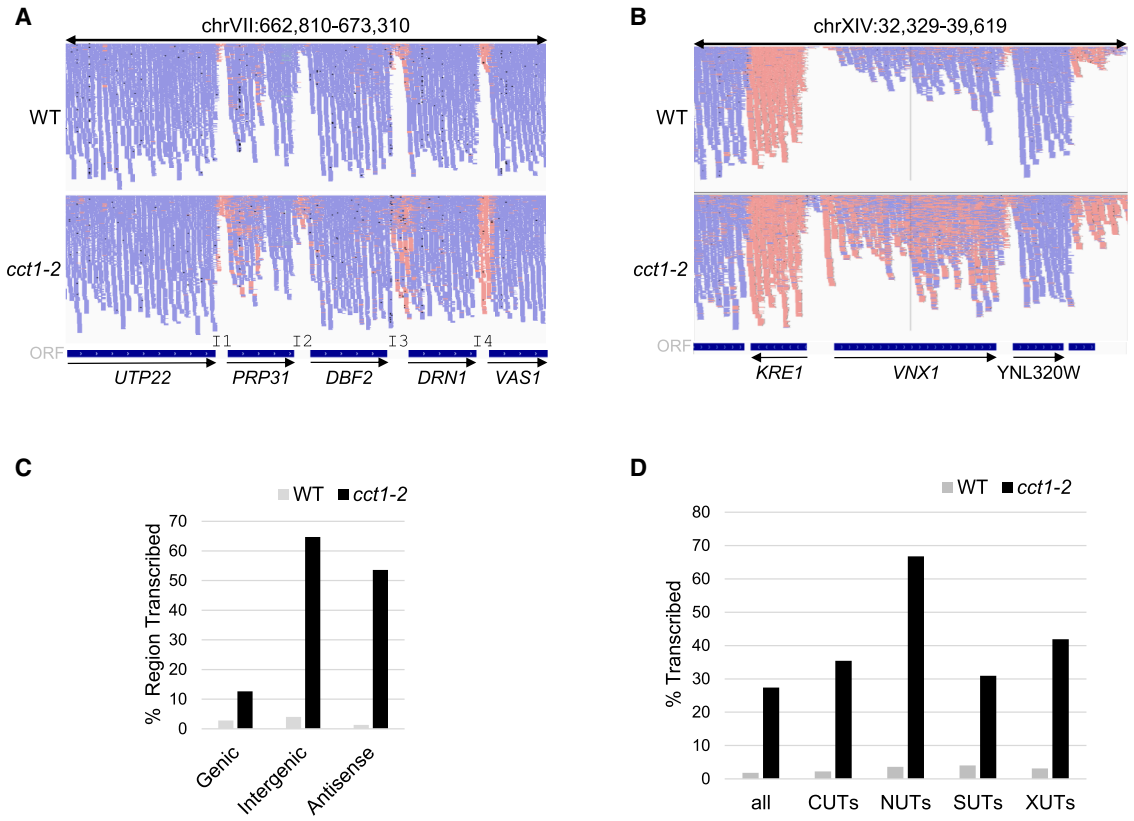

Figure 2. Inactivation of TRiC leads to the accumulation of noncoding RNAs

RNA expression patterns from exponentially dividing wild type (WT) and *cct1-2* yeast exposed to 37°C (non-permissive temperature for *cct1-2*)[41] for 4 h were determined by deep sequencing (RNA-seq) and aligning to the yeast genome.

(A and B) Representative patterns illustrating the accumulation of sequence reads in intergenic areas (A) or antisense RNAs within an open reading frame (B) are shown. The intergenic regions shown in (A) were designated intergenic region 1, 2, 3, or 4 (I1, I2, I3, I4).

(C) TRiC inactivation correlated with a biased increase in the accumulation of cryptic (intergenic and antisense) RNAs.

(D) The relative representation of aberrant RNAs in WT and *cct1-2* yeast exposed to 37°C for 4 h is shown for known cryptic unstable transcripts (CUTs), Nrd1-unterminated transcripts (NUTs), stable unannotated transcripts (SUTs), and Xrn1-sensitive unstable transcripts (XUTs).

See also Figure S1.

TRiC inactivation triggers accumulation of divergent noncoding RNA transcripts

To start assessing the influence of the TRiC chaperonin on nuclear events, we examined steady-state RNA transcripts in the presence and absence of active TRiC. To inactivate TRiC, we used the temperature-sensitive strain *cct1-2* (G423D), which is fully active at the permissive temperature (30°C) and inactivates at 37°C (Figure S1A).[12,41] We exploited an established temperature regime of 4 h at 37°C, which prompts cessation of cell growth that is reversible following return to a permissive temperature.[41] In brief, exponentially growing parental (wild type [WT]) and *cct12* yeast were shifted to 37°C for 4 h; RNA was isolated, and RNA-seq analysis was performed. The most apparent phenotype was the emergence of noncoding/cryptic RNA transcripts including the accumulation of RNAs from bidirectional promoter firing (Figures 2A, I1, I2, I3, and I4, and S1B) and rise in antisense RNAs across open reading frames (Figures 2B and S1C). Of note, there was no apparent correlation between the affected loci and whether these genes were regulated by known TRiC substrates SAGA or TFIID (data not shown).[42]

While there were changes to steady-state genic RNAs, these were relatively minor with 71 up-regulated (2-GFold; GFold threshold of 0.01)[43] and 85 down-regulated (50%) genes out of the 6,692 yeast open reading frames (ORFs). In general, the activated genes (35/71) were linked to stress response/protein folding, and the repressed genes (51/71) were associated with the ribosome/translation. Basically, the changes in sense transcript levels were comparable to a mild stress condition (Figure S1D).[44] Contrasting the limited changes in ORF sense RNAs, loss of TRiC had a large influence on the steady-state levels of cryptic RNAs (i.e., any RNA not representing sense RNA of an ORF) (Figure 2C). In addition to the *cct1-2* temperature-sensitive mutant, we observed a comparable, albeit weaker, transcription response using the milder *ts* variant *cct4-1* (G345D) (Figures S1E and S1F).

To evaluate the RNAs accumulating in *cct12* at 37°C, normalized RNA-seq reads along the entire genome were compared

from WT and *cct1-2* samples at each nucleotide position. We developed a computational script (interval identifier) for the comparison that uses normalized RNA-seq nucleotide coverages to identify intervals with at least a 4-fold differences in read counts (Figures S1G and S1H). An advantage of interval identifier is that the length of the area with differential coverage between comparison datasets (e.g., parental vs. mutant) depends on the continuity of a 4-fold difference between the adjacent nucleotides. At a threshold where *cct1–2* read counts were increased ≥4-fold relative to parental (*cct1-2*/WT), ∼9.8% of the genome was associated with noncoding RNAs following TRiC inactivation. In contrast, only ∼0.3% of the genome showed a ≥4-fold increase in parental read counts compared to *cct1-2* (WT/*cct1-2*). For noncoding transcripts, the parental RNA pool covered ∼4% of the upstream intergenic region while *cct1-2* coverage increased to ∼65% of the total intergenic areas. In addition to promoter-associated RNAs, 51 ORFs displayed a substantial change in the directionality of transcript production following loss of TRiC (Figures 2B and S1C). Apart from these noncoding RNAs (i.e., bidirectional promoter transcripts and antisense ORF RNAs), there were no clear reference points for where the rest of the cryptic RNAs started and ended since the locations and intensities varied with respect to gene bodies and intergenic regions.

To determine if the diversity of transcripts that are produced in the absence of active TRiC represented known cryptic RNAs, we compared the *cct1–2* pool to previously identified aberrant RNA classes including cryptic unstable transcripts (CUTs), stable unannotated transcripts (SUTs), Xrn1-sensitive unstable transcripts (XUTs), and Nrd1 unterminated transcripts (NUTs). First, we analyzed an established NUT dataset using interval identifier and found that it successfully recognized cryptic RNAs (Figure S1G). Next, we analyzed the WT and *cct1-2* RNA-seq datasets with interval identifier and compared the results to previous reports on CUTs, SUTs, XUTs, and NUTs.[45–48] The *cct1-2* RNAs overlapped with ∼35% of CUTs, ∼31% SUTs, ∼42% XUTs, and ∼67% NUTs (Figure 2D). Collectively, the known pool of CUTs, SUTs, XUTs, and NUTs covered ∼15% of the *cct1-2* cryptic transcriptome. The changes in these noncoding RNA levels suggest that a TRiC-dependent breakdown in the RNA quality control process accounts for much of the stable cryptic transcripts present in *cct1-2* cells.

To check whether TRiC is involved with a known RNA quality control component, we examined sites associated with the RNA quality control factor Nrd1. Studies on Nrd1 have shown that it is involved in many classes of aberrant nuclear RNAs and is therefore a key constituent for the global surveillance of the transcriptome.[48,49] Since the binding motif for Nrd1 is enriched in snoRNAs,[48] we examined these loci. In general, snoRNA encoding genes displayed increased readthrough beyond the transcription termination sites (Figure S1I, I5 and I6). For almost half of the snoRNA genes (30 out of 68), the level of readthrough transcripts was ∼1.5-fold higher in *cct1-2*, yet the level of RNA prior the termination site was comparable (Figure S1J). Readthrough transcripts were also apparent at the non-snoRNA gene, *SNU56*, which is also targeted by Nrd1 (Figure S1K). Of note, divergent RNAs from read through of *SNU56* and from bidirectional promoter firing of YDR239C are both present in intergenic region I7 (Figure S1K). All of these loci displayed a mild decline in Nrd1 occupancy at the 3′ ends as measured using the chromatin immunoprecipitation (ChIP) assay (Figure S1L). Yet, given the difference in the magnitude of the cryptic RNA phenotype vs. the mild change in Nrd1 occupancy, we concluded Nrd1 impairment does not explain the observed RNA changes occurring after TRiC inactivation. We therefore explored the influence of TRiC on other nuclear pathways including chromatin-associated features.

Influence of TRiC on epigenomic marks

The TRiC chaperonin has been linked to numerous chromatin modifiers including SAGA, NuA4, RPD3S/L, SET3C, SET1C, HDA1, HST3/4, and SPT10.[31–35,50] TRiC is minimally needed for the proper assembly of the SMRT-HDAC3 and TFIID complexes.[18,36] We therefore examined whether TRiC has an active role in modulating the epigenomic and chromatin landscapes and if this could account for the large increase in steady-state cryptic RNAs. Using standard procedures, we isolated histones from exponentially growing parental (WT) and *cct1-2* cells incubated for 4 h at 37°C and interrogated 23 different histone post-translational modifications (PTMs) by mass spectrometry.[51]

Perhaps unexpectedly, the only observed significant change to the histone code was an ∼25% (±8% SD) increase of H3K79me3 in *cct1-2* cells (Figures 3A and S2A–S2C). The H3K79me3 PTM often demarcates nucleosomes at or near actively transcribed loci, and H3K79me3 has been implicated in pervasive extragenic transcription.[52–54] Of note, ∼29% of the sites displaying increased steady-state transcripts in *cct1-2* overlapped with established H3K79me3 peaks (data not shown).[54] We did find a small increase in H3K79me3 at sites subject to elevated cryptic transcripts (Figure 3B). However, not all sites with cryptic RNAs correlated with elevated H3K79me3 levels (Figure 3B, I8 and I10). The disparity in the magnitude of the TRiC-dependent differences between epigenomic changes and the increased levels of cryptic RNAs upon TRiC inactivation suggests that other/additional factors contribute to the accumulation of the noncoding RNAs.

As H3K79me3 has been reported to be mutually exclusive with the H2A.Z histone variant,[55,56] we examined the correlation between H2A.Z and pervasive RNA production. We found that H2A.Z occupancy declined ∼2-fold at sites having elevated divergent RNAs in *cct1-2* (Figure 3C). The reduction in H2A.Z chromatin occupancy occurred in a time-dependent manner after TRiC inactivation (Figure S2D). Of note, the TRiC-dependent decrease in H2A.Z chromatin association appears to be independent of H3K79me3 since a similar change in H2A.Z occupancy was observed in *dot1*Δ yeast following TRiC loss (Figure S2E)—Dot1 is the lone H3K79 tri-methyltransferase in yeast.[57]

We found that the steady-state levels of the H2A.Z protein declined in *cct1-2* at the restrictive temperature with no apparent change in H3 protein (Figure 3D), which suggests that the H2A.Z protein relies on the TRiC chaperonin for stability, as is typical for a chaperonin substrate. Of note, deletion of the H2A.Z encoding gene *HTZ1* further sensitized *cct1-2* yeast to increased temperature, thereby showing a physiological link between these factors (Figure S2F). Given the connections between TRiC and

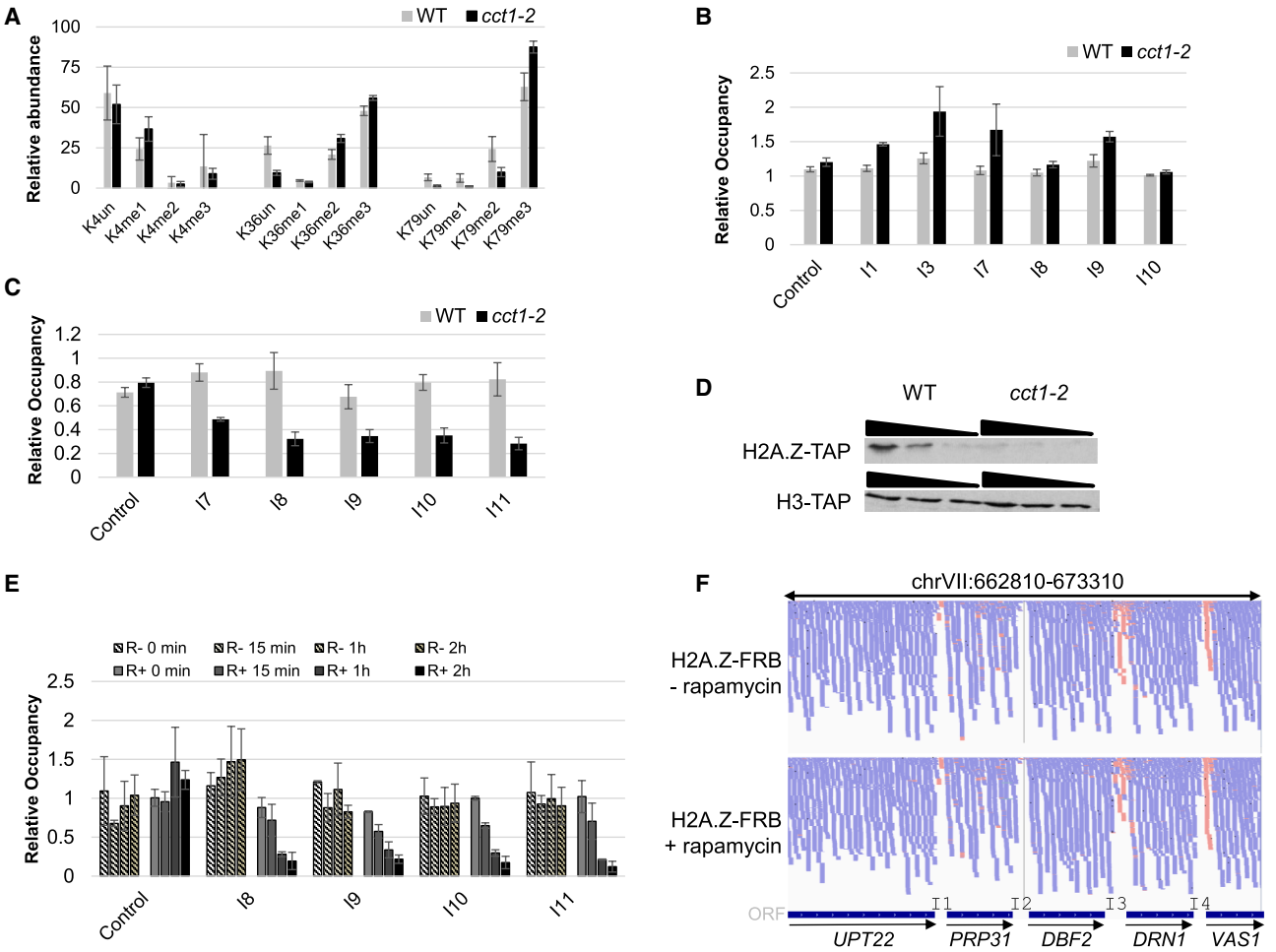

Figure 3. TRiC influence on histone modifications and correlation to cryptic RNAs

(A) Mass spectrometry analysis of histone tail post-translation modifications was performed on histone proteins that were isolated from exponentially dividing WT and *cct1-2* yeast exposed to 37°C for 4 h. The relative abundance of select H3 modifications are shown as mean ± SEM.

(B) The relative levels of H3K79me3 at sites associated with H2A.Z occupancy were determined at control (*ACT1*), I1, I3, and I7-I10 and shown as mean ± SEM.

(C) The relative chromatin occupancy of H2A.Z was determined and represented as mean ± SEM at control (*ACT1*) and I8-I11 sites in WT and *cct1-2* yeast engineered to express H2A.Z as a TAP-tagged fusion.

(D) The steady-state levels of H2A.Z-TAP and H3-TAP, as indicated, were checked in WT and *cct1-2* yeast exposed to 37°C for 4 h by immunoblot analysis using an α-TAP antibody and titrations of whole cell extracts (100, 50, and 25 μg).

(E) Using the anchor-away assay, H2A.Z was depleted from the nucleus in engineered WT yeast. The relative chromatin occupancy of H2A.Z at control (*ACT1*), I8-I11 was checked by ChIP following addition of DMSO (striped bars) or rapamycin (open bars) at the indicated time points, where the bars represent mean ± SEM.

(F) The impact of H2A.Z nuclear depletion on RNA patterns was determined using anchor away and RNA-seq. Yeast were treated with DMSO or rapamycin for 2 h; cells were collected; isolated RNA was deep sequenced, and reads were aligned to the yeast genome.

See also Figures S2 and S3.

H2A.Z, we tested if a reduction of H2A.Z at gene promoters instigated an accumulation of cryptic RNAs comparable to TRiC inactivation. To trigger the loss of H2A.Z in chromatin, we engineered an H2A.Z anchor-away yeast strain. In brief, anchor away allows the controlled removal of a protein from the nucleus by taking advantage of the Rapamycin-dependent interaction between FKBP12 and the FKBP Rapamycin-Binding domain (FRB) of TOR1 in addition to the flow of ribosomal proteins from the nucleus to the cytoplasm.[58] Following rapamycin addition, we observed a time-dependent depletion of H2A.Z from chromatin as measured by ChIP (Figure 3E). Despite the H2A.Z reduction, there was no significant change in the accumulation of divergent RNAs, as determined by RNA-seq (Figure 3F). Overall, these experiments indicate that H2A.Z is likely a substrate of TRiC, yet the TRiC-dependent loss of H2A.Z does not account for the increase in steady-state levels of cryptic transcripts upon TRiC inactivation.

Our prior work on the roles of molecular chaperones in the nucleus showed that both Hsp90 and p23 impact chromatin accessibility.[59–61] Hence, we evaluated whether the TRiC chaperone might have a similar influence by mapping the global DNaseI hypersensitivity sites (DNaseI-seq).[59,62] We observed that TRiC

does not modulate the total quantity of open chromatin regions across the genome. The number of DNaseI hypersensitive sites (DHSs) was comparable following TRiC inactivation (parental DHSs = 4,520 and *cct1-2* DHSs = 4,492). Yet, there were changes to the locations of the DHSs (~20% of parental DHSs are lost at the restrictive temperature with an ~16% gain in DHSs specific to the *cct1-2* background) (Figure S3A). Also, the average DHS *Z* score, which is a measure of DNase I cleavage level,[63] reduced from 19.5 in parental cells to 13.2 in *cct1-2* (32% reduction), indicating a mild reduction in chromatin accessibility following loss of TRiC (Figure S3B). These experiments demonstrate that TRiC can influence chromatin accessibility since access was reduced mildly. Yet, the changes in DHSs (i.e., decreased size, increased, or unique to background) did not correlate with the production of cryptic RNAs (Figure S3C). For example, ~50% of the divergent RNAs associated with bidirectional promoter firing did not display a change in accessibility. To this point, we conclude that the observed increases in cryptic RNAs following TRiC inactivation are not accounted for mechanistically by changes in RNA quality control, histone modifications, or chromatin accessibility.

Inactivation of TRiC triggers a significant increase in nascent RNA production

We next focused on the possible role of TRiC in the process of RNA biogenesis. The steady-state levels of any RNA transcript is set by multiple events including RNA synthesis and decay pathways.[64] To evaluate the global dynamics of nascent transcript production, we exploited metabolic labeling of RNA with the nucleotide analog 4-thiouracil (4tU) followed by high-throughput sequencing (4tU-seq).[65,66] In brief, 4tU-seq allows the relative contributions of synthesis and decay rates to steady-state RNA levels to be appraised.[66] Hence, we evaluated nascent RNAs in parental and *cct1-2* cells using 4tU-seq.

Following a 4 h incubation at 37°C, parental and *cct1-2* cells were exposed to 4tU for 5 min to label the nascent transcripts. RNA isolated from labeled and unlabeled (control) cells were conjugated to biotin with a thiol-reactive reagent; the biotinylated RNA was affinity purified with streptavidin, and the isolated RNA was sequenced. Notably, we observed a dramatic increase in nascent RNA production in *cct1-2* yeast (Figures 4A and S4). At a threshold of ≥4-fold for *cct1-2*/WT, ~22.8% of the genome displayed higher levels of nascent RNAs. whereas only ~0.4% of the genome had levels ≥4-fold when comparing WT to *cct1-2*. Relative to the steady-state RNAs (Figure 2), nascent transcripts cover more of the genome (~9.8% vs. 22.8%) and are ~7.3-fold more abundant. In contrast to the biased changes in intergenic and antisense transcripts within the steady-state RNA pool of *cct1-2* (Figure 2), the nascent RNAs were elevated across the genome in *cct1-2* (Figure 4B). As might be anticipated, given the broad genomic expression pattern of the *cct1–2* transcripts, the *cct1–2* nascent RNAs overlapped well with all classes of known cryptic RNAs including CUTs, SUTs, XUTs, and NUTs (data not shown). Thus, the increased production of nascent RNAs is contributing to the accumulation of noncoding RNAs.

In addition to evaluating nascent RNA production, the 4tU-seq data in conjunction with RNA-seq can be used to gauge RNA degradation rates.[65,67] In brief, RNA half-lives are proportional to the normalized number of RNA molecules (RNA-seq) divided by the level of normalized, actively produced RNAs (4tU-seq). Analysis of the parental (WT) and *cct1-2* datasets revealed that the WT RNA pool has longer-lived transcripts (i.e., parental pool has higher levels of RNA species with a half-life estimator value of ≥4), and shorter-lived transcripts are preferentially found in *cct1-2*; accordingly, the *cct1-2* pool is enriched for RNAs with half-life estimator values ≤ 4 (Figure 4C). Hence, the loss of TRiC resulted in an increased production of nascent RNAs but also shortened the RNA lifespan. Likely, the increased degradation rate is the cell's attempt to restore RNA homeostasis by countering the increased production rate of nascent RNAs. We suspect that the increase of cryptic RNAs in the steady-state pool (Figure 2) resulted from preferential activity of the RNA quality control machinery on coding RNAs, which would reduce the stable output of coding RNAs to near normal but prolong the lifetime of noncoding RNAs. This could be due to either RNA quality control being overwhelmed by the increased level of substrate or by a preferential recognition of coding RNAs. Regardless of the mechanism, these experiments indicate that a major outcome of TRiC loss is the increase in the global production of RNAPII-dependent nascent RNAs.

Nuclear depletion of TRiC triggers increased noncoding RNA accumulation

We assessed if the effect of TRiC loss on RNA transcript production involves its cytoplasmic locale or whether it is due to a nuclear role of TRiC. Initially, we attempted to use the anchor-away approach to remove TRiC from the nucleus but, unfortunately, our attempts to use various TRiC subunits as FRB fusions in anchor away were unsuccessful (Figure S5A). Instead, we exploited our existing Cct2-GFP and Cct6-GFP strains and transformed these cells with a *GAL1*-driven expression vector for a GFP nanobody that also has 3 nuclear export signals (NES-GFP-Nanobody). Following the addition of galactose to the media, we found a time-dependent nuclear depletion of Cct2-GFP or Cct6-GFP and correlative increases in steady-state intergenic RNAs but not genic (Figures 5A, 5B, and S5B). Importantly, the cytosolic function of TRiC remained intact as the levels of actin and tubulin remained constant (Figure S5C). While the impact on RNA levels was not as sizeable as that observed in *cct1-2* (Figures 2A and S1B), our nanobody depletion tactic only reduced nuclear levels by ~50% (Figure 5C), which might account for the lower influence on transcript production. Despite only reducing its nuclear presence by ~50%, these strains had mild growth defects suggesting that depletion of nuclear TRiC impacts cell viability (Figure S5D). Intriguingly, a closer examination of TRiC in the depleted nuclei revealed a punctate staining pattern for the remaining nuclear TRiC that colocalized with RNAPII signal (Figures 5D and S5E). We speculate that as nucleoplasmic TRiC is depleted, a recycling factor needed to disengage TRiC from the DNA-bound RNAPII is removed (e.g., the open-state cofactor PDCD5 [yeast homolog is Sdd2]).[68] Minimally, normal amounts of nuclear TRiC are required to maintain proper levels of RNA including in the balance of intergenic and genic species.

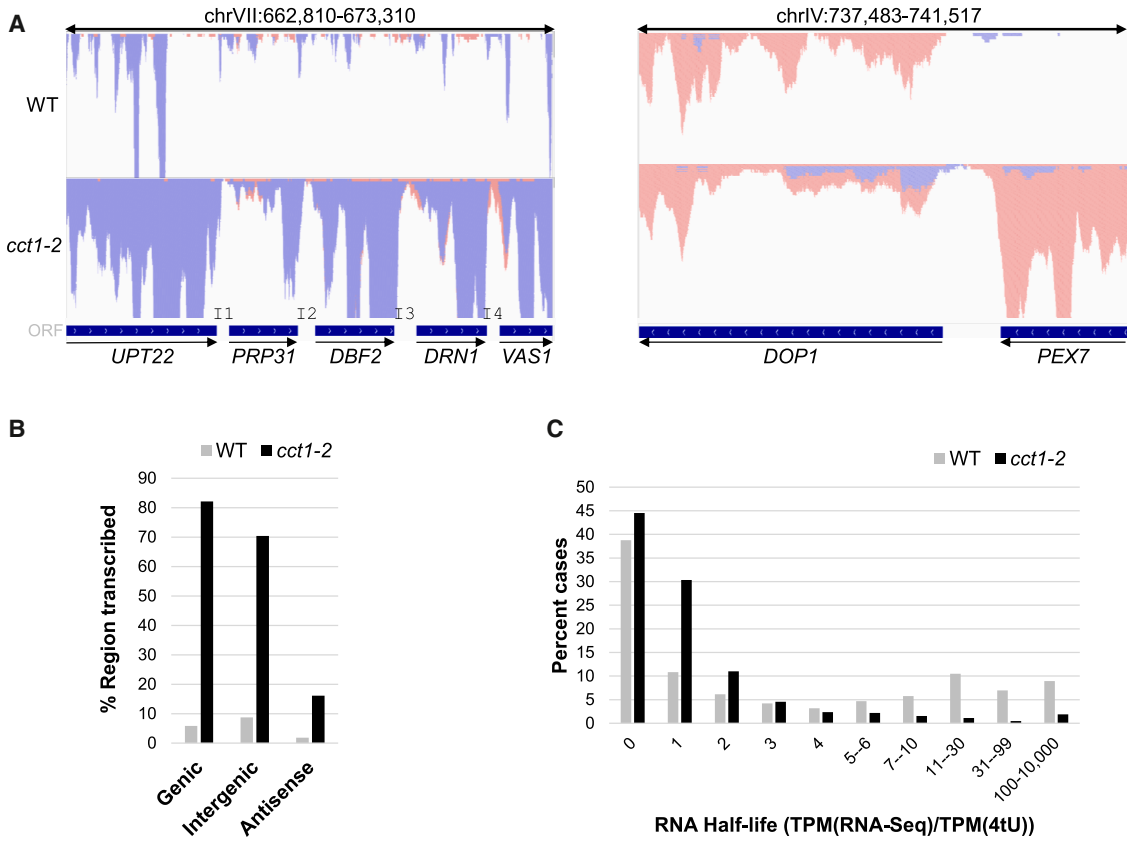

Figure 4. Production of nascent RNAs is TRiC dependent

(A) The relative levels of active transcription in exponentially dividing WT and *cct1-2* yeast exposed to 37°C for 4 was monitored by 4tU-seq. For illustrative purposes, 2 different areas of the genome are shown with the sequences reads aligned to the yeast genome from samples prepared from WT or *cct1-2* yeast exposed to 37°C for 4 h.

(B) TRiC inactivation increased the production of nascent RNA transcripts across the genome regardless of RNA type (i.e., genic, intergenic, or antisense).

(C) Relative RNA half-lives in WT and *cct1-2* cells exposed to 37°C for 4 h were calculated as TPM(RNA-seq)/TPM(4tU-seq) where TPM is transcripts per million. See also Figure S4.

TRiC directly regulates RNAPII activity

Given the established chaperonin role of assembling/disassembling macromolecular complexes, we assessed whether TRiC-regulated RNAPII by altering the composition of the RNAPII structure. We performed TAP-tag isolations of the RNAPII complex using strains expressing the largest subunit, Rpb1, as a TAP fusion in the WT or *cct1-2* backgrounds. Following a standard 2-step TAP purification, no differences in RNAPII subunit levels were apparent (Figure 6A). To detect TRiC association, we had to use less-stringent conditions. We pulled down the TAP-tagged polymerase complex using a 1-step procedure followed by immunoblot analysis to visualize the Rpb1-TAP and TRiC proteins. While equivalent levels of Rpb1 were isolated, the levels of TRiC increased ~2-fold in the *cct1-2* pulldown sample (Figure 6B). Of note, comparable pulldown experiments using extracts prepared from cells not expressing a TAP-tagged Rpb1 fusion did not detect any bead-associated TRiC (data not shown).

Since TRiC is associating with the assembled RNAPII complex, we checked whether the chaperonin is influencing polymerase function by performing *in vitro* transcription assays. We prepared standard nuclear extracts from cells treated for 4 h at 37°C and evaluated the *in vitro* production of RNA from the *VAS1* promoter, which displayed increased noncoding RNA levels associated with bidirectional promoter firing *in vivo* (Figures 2A, 4A, 5B, and S4). The biotinylated *VAS1* promoter DNA template was immobilized on magnetic beads, and the bidirectional production of RNAs from the *VAS1* transcription start site (TSS) was visualized by standard primer extension assays with oligonucleotides select for upstream or downstream RNAs. The *VAS1* promoter fired pervasively producing transcripts in an orientation-independent manner with the *cct1-2* nuclear extract creating ~10-fold more RNA in both directions (Figure 6C). Titration of purified, recombinant TRiC into the *cct1-2* nuclear extract was sufficient to reduce the activity of RNAPII, in a dose-dependent manner, to the level of RNAPII in WT nuclear extract (Figure 6C). We further used the biotinylated DNA template to assess the levels of associated TRiC and found that the *cct1-2* TRiC had enhanced interactions with DNA-engaged RNAPII (Figure 6D). The WT

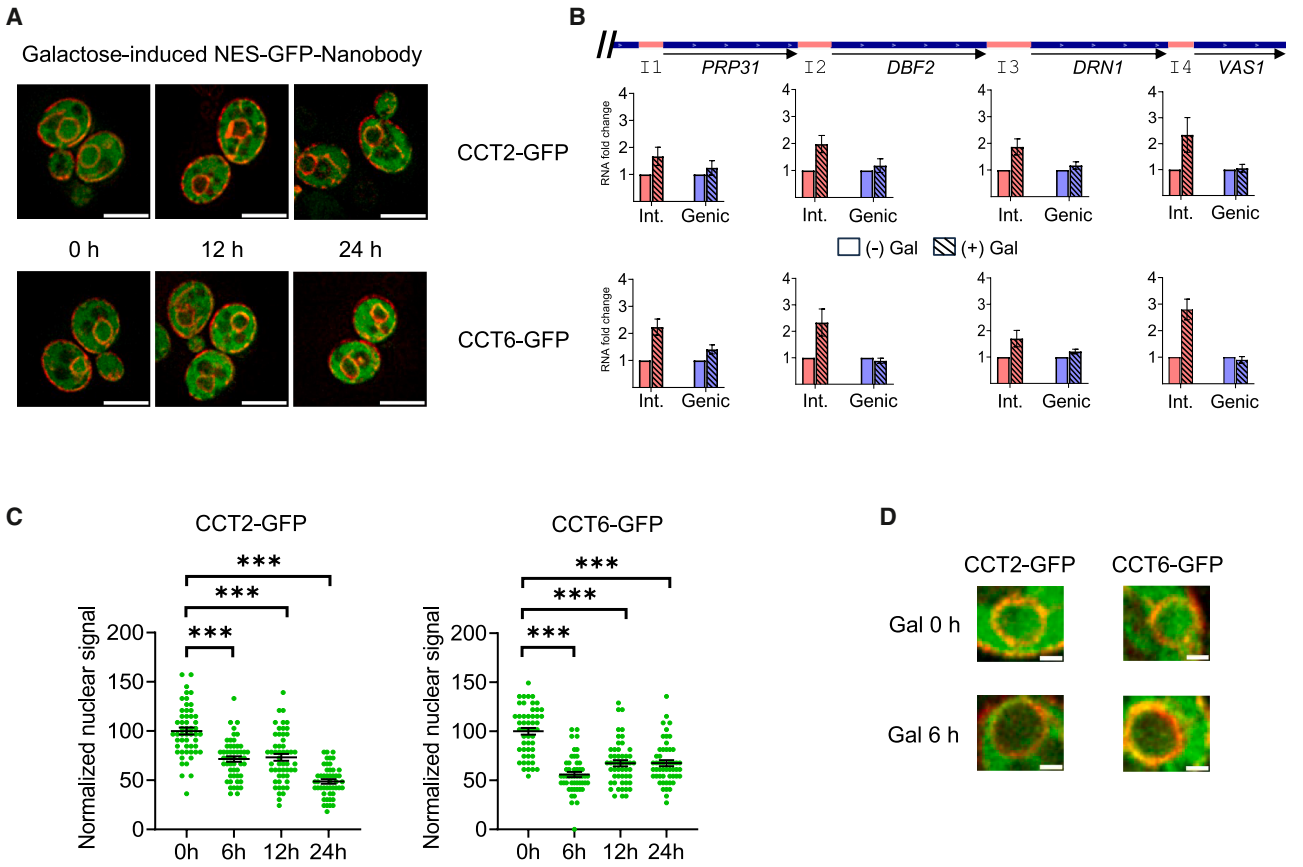

Figure 5. Active nuclear export of TRiC depletes the nucleoplasm but leaves the chromatin-associated chaperonin

(A) The cellular localization of TRiC was visualized using yeast expressing the Cct2 or Cct6 subunit as a GFP fusions and a mCherry-Pho88 fusion to mark the outer and nuclear membranes.[40,69] The yeast transformants also carried an expression vector for a GFP-Nanobody with nuclear export signals (3× NES) under the control of the *GAL1* promoter. To trigger nuclear depletion of TRiC, yeast growing exponentially in selective simple raffinose-based media were supplemented with galactose. The GFP signal was visualized at 0, 12, and 24 h post galactose addition with confocal images acquired using a DeltaVision OMX.

(B) Yeast expressing GFP fusions of either Cct2 or Cct6, as marked, were transformed with the NES-GFP-Nanobody. Exponentially growing cells were supplemented with galactose, incubated for 24 h, and RNA was isolated. The production of intergenic (Int.) or genic (Genic) RNA was monitored by reverse-transcription quantitative PCR (RT-qPCR) using select primers. The normalized intergenic signal is represented by pink bars and normalized genic signal by blue bars as mean ± SEM.

(C) The relative depletion of the Cct2-GFP and Cct6-GFP, as marked, signal from the nucleus was monitored before and after galactose addition to trigger expression of the GFP-NES-Nanobody. GFP signals were normalized to total intensity of each cell, and the values at the indicated time points were quantified and graphed as mean ± SEM. Statistical analysis used Student's *t* tests (p value < 0.05 cutoff) with $n = 6$ (50 cells each) for all quantifications with ***$0.0001 < p < 0.001$.

(D) Representative images of the nuclei of cells expressing CCT2-GFP or CCT6-GFP, as marked, before (Gal 0 h) or after addition of galactose (Gal 6 h) are shown. The images were acquired using a DeltaVision OMX.

See also Figure S5.

and *cct1-2* reactions were prepared using a DNA template master mix. Intriguingly, inactivation of TRiC using the *cct1-2* allele also prompted increased interaction of TRiC with the chromatin fraction in a cell fractionation assay (Figures 6E and S6A). Hence, WT TRiC is present in both the nucleoplasm and bound to the chromatin. Heat treatment of the *cct1-2* cells stabilized the chaperonin to RNAPII in the chromatin fraction.

As a prior study had suggested that the *cct1-2* mutation disfavored substrate binding using the folding targets actin and tubulin,[12] our observations compelled a follow-up evaluation of TRiC-substrate interactions in the WT and *cct1-2* backgrounds. In brief, we wished to assess whether TRiC binding to RNAPII differs from the well-established substrates actin and tubulin.[12] We employed yeast cells expressing the Cct6 subunit as a Calmodulin binding protein (CBP) fusion where the CBP tag was placed in a flexible surface linker of Cct6 that is known to not interfere with substrate protein interactions.[40,70] Using calmodulin beads, we isolated the TRiC complex from WT and *cct1-2* cells. Significantly, the *cct1-2* TRiC was associated with elevated levels of the RNAPII complex and the known chaperonin substrates actin and tubulin (Figures 6F and S6B). As the prior study used an amino-terminal hemagglutinin (HA) tag on the amino-terminus of the Cct2 subunit and terminal tags are known to be buried within the substrate-binding cavity of chaperonins,[70,71] we suspect that the combination of the amino-terminal tag and *cct1-2* mutation resulted in destabilization of substrate interactions; in contrast to our use of an internal using an epitope tag in a flexible

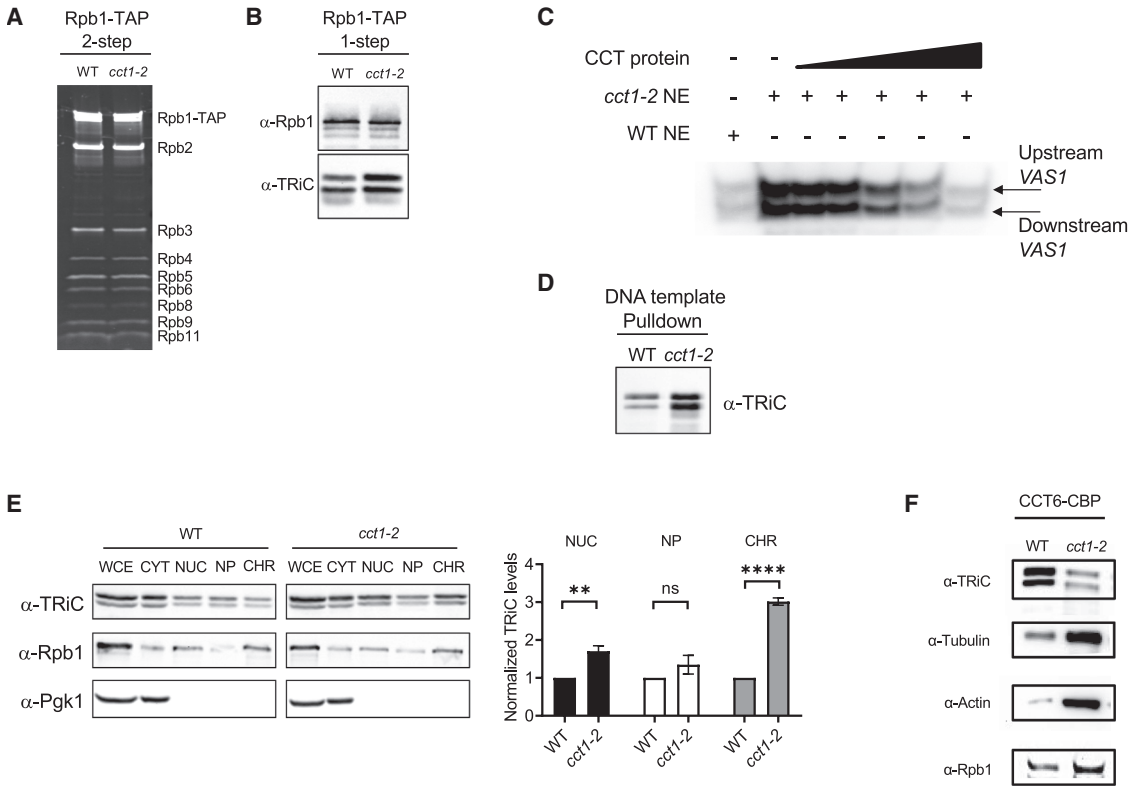

Figure 6. TRiC directly regulates RNA polymerase activity

(A) Using the standard 2-step tandem affinity pulldown assay RNAPII complexes were isolated from extracts prepared from TAP-RPB1 parental or TAP-RPB1 *cct1-2* yeast, resolved by SDS-PAGE, and the indicated RNAPII subunits were visualized using Sypro RUBY (Invitrogen).

(B) RNAPII complexes were isolated using a 1-step TAP pulldown from extracts prepared from TAP-RPB1 parental or TAP-RPB1 *cct1-2* yeast, resolved by SDS-PAGE, and the Rpb1 or TRiC subunits were visualized by immunoblot analysis using either an α-TAP or α-Cct1/3/6 (α-TRiC) antibody, respectively.

(C) *In vitro* transcription reactions were performed using nuclear extract (NE) prepared from exponentially dividing WT or *cct1-2* yeast exposed to 37°C for 4 h, as marked. The *cct1-2* NE was supplemented with purified, recombinant TRiC (5, 10, 25, 50, and 100 nM final), as indicated. The production of genic (downstream *VAS1*) or intergenic (upstream *VAS1*) RNA was detected by primer extension using select oligonucleotides.

(D) Equal amounts of WT and *cct1-2* NE (100 μg) were incubated with biotinylated-promoter DNA, washed, boiled in SDS sample buffer, resolved by SDS-PAGE, and the DNA-associated or NE TRiC was visualized by immunoblot analysis using an α-TRiC antibody.

(E) Parental (WT) or *cct1-2* yeast were heat treated for 2 h at 37°C, and the cells were fractionated into whole cell extract (WCE), cytosolic (CYT), nuclear (NUC), nucleoplasm (NP), and chromatin (CHR). The relative levels of TRiC in each fraction were determined by immunoblot analysis using an α-TRiC antibody. α-Pgk1 was used a control marker for the cytosol, and α-Rpb1 was the marker for the nucleus, as indicated. The relative levels of TRiC in a biological triplicate of the nuclear-associated fractions was determined, quantified, and graphed as mean ± SEM. Statistical analysis used Student's *t* tests (p value < 0.05 cutoff) with $n = 4$ for all quantifications with $^{**}0.001 < p < 0.01$ and $^{****}p < 0.0001$.

(F) Yeast expressing the Cct6 subunit as a CBP fusion in the parental (WT) or *cct1-2* backgrounds were heat treated for 4 h at 37°C, and TRiC was isolated using calmodulin beads. The relative levels of TRiC and the bound substrates tubulin, actin, and RNAPII were determined by immunoblot analysis using α-TRiC, α-tubulin, α-actin, and α-Rpb1 antibodies, as marked.

See also Figure S6.

linker of Cct6, which neither interferes with substrate binding nor folding.[40,71] Taken together, our results demonstrate that TRiC directly controls the activity of RNAPII to achieve a normal transcriptional output that is important to achieve RNA homeostasis in the nucleus.

Expression of the TRiC substrate Htt disrupts RNAPII interaction and regulation

Our work supports a model in which the TRiC chaperonin regulates the general transcriptional activity of RNAPII. As TRiC is commonly recognized as a central molecular chaperone, we examined whether the TRiC:RNAPII association connects the proteostasis and transcription pathways. We exploited the known TRiC substrate Huntingtin protein (Htt) for this purpose. Htt is widely expressed and involved in a number of biological pathways including intracellular transport and autophagy.[72] Significantly, expansion of a polyglutamine (polyQ) repeat within Htt correlates with the development of Huntington's disease (HD).[73] HD is a progressive and disabling neurodegenerative disorder impacting the central nervous system of ~1 in 10,000 people. Aggregation of the polyQ-expanded Htt correlates with altered gene programs and collapsed proteostasis.[74,75] Whether these two phenomena might connect was previously not understood.

We expressed the HD Htt variant Q103 in normal yeast cells as a GFP fusion (HttQ103-GFP). As a first step, we checked if the galactose-induced expression of HttQ103-GFP altered the steady-state levels of the RNAPII subunit Rpb1, TRiC subunits Cct1/3/6, and the cochaperone Sba1 and observed no significant changes (Figure 7A). In general, the HttQ103-GFP localized throughout the cells (Figure 7B). Pulldown experiments showed that Rpb1-TAP had a lowered interaction with TRiC and that HttQ103-GFP was associated with the chaperonin (Figures 7C and 7D). Significantly, the levels of steady-state RNA, both intergenic and genic, declined following expression of HttQ103-GFP, as determined by reverse-transcription quantitative PCR (RT-qPCR) analysis of isolated RNA (Figure 7E). The genic RNA for DBF2 was an exception, which may reflect the biological role of Dbf2 since it encodes for a kinase that responds to both transcription and physiological stress.[76] Minimally, our data demonstrate that expression of the HD variant and known TRiC substrate HttQ103 correlates with reduced TRiC RNAPII association and altered RNAPII activity.

DISCUSSION

A central feature of proteostasis is the recognition and manipulation of protein conformations by molecular chaperones to support and regulate substrate form and function.[77] Typically, the emphasis is on nascent polypeptide biogenesis and damaged protein triage. However, chaperones also regulate the activity of mature cellular proteins thereby conferring a mechanism for recurrent protein regulation.[78,79] Here, we show that nuclear TRiC is required to modulate RNAPII activity, thereby maintaining a proper level of transcriptional output and balance RNA homeostasis. Although we do not delineate the structural mechanism by which TRiC controls RNAPII activity, our study shows that TRiC contributes to RNA homeostasis by modulating the output of RNAPII. As RNAPII is reiteratively used to produce RNA transcripts, cycling this enzyme complex through a central molecular chaperone (i.e., TRiC chaperonin) could link the proteostasis process to the production of RNA transcripts. Our data suggest that TRiC serves as an RNAPII rheostat, conferring a persistent regulatory influence based on chaperonin availability. Under conditions where TRiC activity is occupied with protein substrates, the production of RNAPII transcripts would decrease. For instance, when the folding process is overburdened because TRiC is heavily engaged supporting substrates including when cells are under physiological stress such as heat shock or aging. In our model, TRiC is a key determinant for balancing proteostasis and mRNA production.

Classically, the regulation of proteins by a chaperonin is thought to occur within the inner cavity of the 2 stacked rings forming the TRiC structure.[1] As the size limitation of this folding chamber is ~70 kDa, this raises an obvious concern on how TRiC might regulate the >500 kDa RNAPII complex. Yet, TRiC has been shown to facilitate the folding of proteins larger than 70 kDa including the ~110 kDa spliceosome subunit Snu114 where TRiC partially encapsulates the carboxyl-domain of Snu114 to prompt its folding, while the amino-terminal domain is independent of TRiC.[80] Hence, TRiC may regulate RNAPII as a folding substrate by engaging a protruding domain of a subunit of the assembled RNA polymerase enzyme complex.

It was unexpected to find that the classic TRiC temperature-sensitive mutant *cct1-2* stabilized the chaperonin to the RNAPII complex and fostered a heightened transcriptional output of polymerase (Figures 2, 5, and 7). How a prolonged TRiC-RNAPII interaction leads to an increased enzymatic activity of RNAPII is not clear. Likely, given that it involves a chaperonin, a conformational change of either the RNAPII complex or at least one of the subunits is involved. It will be pertinent for future work to unravel how this occurs. Perhaps of note, in bacteria, the loss of the omega subunit leads to a long-term association between bacterial RNAP and GroEL.[39] Hence, the chaperonins may have evolved to regulate/support the conformational status of the RNA polymerase machinery. Notably, the presented work suggests TRiC has additional nuclear roles including in the regulation of epigenetic changes and the folding and/or stabilization of H2A.Z. Our study thus establishes TRiC as a regulator of nuclear homeostasis.

Significantly, TRiC/CCT dysregulation has been linked to various ailments including numerous cancers, neurodegenerative diseases, myocardial infarction, and Down's syndrome.[81] It had been assumed that any malady manifesting from a TRiC defect would result in a protein health deficiency, yet our work opens the possibility that TRiC shortcomings might trigger transcriptome-related problems. Of note, recent advances have implicated noncoding RNA transcripts as cancer determinants.[82] For example, downstream-of-gene (DoG) noncoding transcripts, which are a class of long noncoding RNAs (lncRNAs), contribute to carcinogenesis and correlate with patient survival.[83,84] Through undefined mechanisms, DoG RNA levels increase in response to physiological stress including heat shock, osmotic stress, and viral infection.[85–88] As all of these conditions can impinge upon TRiC activity,[81] it is intriguing to consider whether the stress-related expression of DoG RNAs is TRiC dependent.

With the onset of genomic research, a myriad of noncoding transcripts, including promoter-associated pervasive RNAs and natural antisense transcripts (NATs), were found in organisms from bacteria to humans.[89,90] In humans, ~55% of all promoters fire bidirectionally with little bias in orientation and ~40% of all ORFs are transcribed in both directions within a cell population.[89] Despite the commonality of divergent RNAs, finding a connection to the TRiC chaperonin was unexpected. Nonetheless, our open investigation into the nuclear roles of TRiC converged on its influence on RNAPII activity (Figures 2, 5, and 6). TRiC inactivation led to the accumulation of different steady-state noncoding RNAs including upstream transcripts consistent with pervasive bidirectional promoter firing, antisense RNAs within ORFs, and read through transcripts (Figures 2 and S1). A major contributing factor to the production of these noncoding RNAs is likely the increased RNAPII activity found in the absence of TRiC both *in vivo* and *in vitro* (Figures 5 and 6). Interestingly, the TRiC-dependent enhanced production of RNA from bidirectional promoter firing showed little orientation bias *in vitro* (Figure 6C). Yet *in vivo* only the noncoding RNA accumulated (Figures 2, 5B, and S1B), suggesting a mechanism to control the rise in protein coding RNAs. Minimally, the act of translating an mRNA is sufficient to destabilize a transcript[91] or, perhaps, an

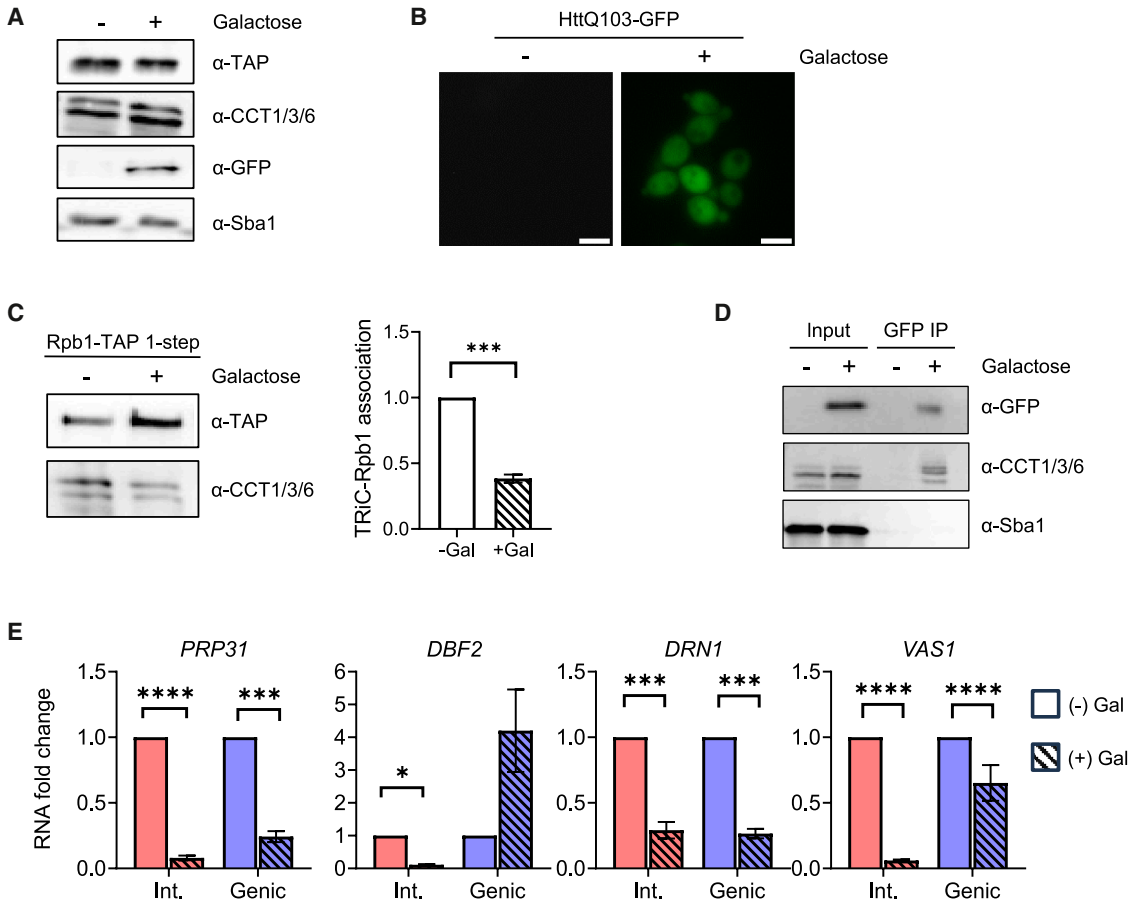

Figure 7. HttQ103 protein competes with RNAPII TRiC association and regulation

(A) Expression of HttQ103-GFP does not influence TRiC or Rpb1 proteins. The relative levels of Rpb1-TAP (α-Rpb1), TRiC (α-CCT1/3/6), HttQ103-GFP (α-GFP), and the loading control Sba1 (α-Sba1) were determined by immunoblot using whole cell extracts prepared from cells expressing Rpb1-TAP and containing a galactose-regulated plasmid for HttQ103-GFP expression grown without (−) or with (+) exposure to galactose (2%).

(B) The cellular localization of HttQ103-GFP was checked by fluorescence microscopy of live cells grown in the absence (−) or presence (+) of galactose by monitoring the GFP signal.

(C) RNAPII was isolated using a 1-step TAP pulldown from extracts prepared from TAP-RPB1 yeast with the GAL1-HttQ103-GFP vector; products were resolved by SDS-PAGE, and the Rpb1 or TRiC subunits were visualized by immunoblot analysis using either an α-TAP or α-Cct1/3/6 (α-TRiC) antibody, as marked. Quantification of biological triplicate pulldowns is graphed as mean ± SEM. Statistical analysis used Student's *t* tests (*p* value < 0.05 cutoff) with $n = 4$.

(D) The interaction between TRiC and HttQ103-GFP was evaluated by immunoprecipitation using an α-GFP antibody. The presence of HttQ103-GFP or TRiC in the pulldown was determined by immunoblot using α-GFP, α-CCT1/3/6, or α-Sba1 (control), respectively.

(E) The impact of HttQ103-GFP on RNA production was measured by RT-qPCR. Yeast containing the *GAL* HttQ103-GFP vector were grown in the absence or presence of galactose (2%); RNA was isolated, and the production of intergenic (red bars) or genic (blue bars) RNAs from the indicated gene loci was monitored by RT-qPCR using select primers and graphed as mean ± SEM. The levels of the ACT1 transcript were to normalize the reactions. Statistical analysis used Student's *t* tests (*p* value < 0.05 cutoff) with $n = 3$ for all quantifications.

additional pathway exists to selectively reduce the levels of coding RNAs to normal. No matter the destabilizing event, we suspect that the increased load of coding RNA is sufficient to saturate the RNA quality control machinery, thereby increasing the lifespan of the observed noncoding RNAs. Overall, our work identifies an important role for the TRiC chaperonin in the control of RNAPII activity in the nucleus to maintain RNA homeostasis.

Limitations of the study

This work supports a model in which the TRiC chaperonin contributes to RNA homeostasis by regulating the output of RNAPII. However, as our experiments cannot distinguish between direct and indirect effects since, we did not incorporate purified components, the precise mechanism by which TRiC is controlling RNAPII activity remains to be determined.

RESOURCE AVAILABILITY

Lead contact

Requests for further information and resources should be directed to, and will be fulfilled by, the lead contact, Brian Freeman (bfree@illinois.edu).

Materials availability

This study did not generate new reagents. All stable reagents used in this study are available from the lead contact without restriction.

Data and code availability

- All imaging and immunoblotting data have been deposited on Mendeley under the 10.17632/z9pd8p875f.2. All DNA-sequencing data have been deposited and are publicly available as of the date of publication. Accession numbers for the RNA-seq, DNaseI-seq, and 4tU-seq are GSE274453, GSE274454, and GSE274455, respectively.
- This paper does not report original code.
- Any additional information required to reanalyze the data reported in this paper is available from the lead contact upon request.

ACKNOWLEDGMENTS

We are grateful to Janhavi Kolhe (UIUC), Lindsey Behrens (UIUC), and Anna Mankovich (UIUC) for their assistance and advice with this work. Funding: B.C.F., Z.G., A.Y.T.P., and A.B. were supported by NIH R35 GM136660; Z.G. was supported by NIH F32 GM140555; K.S. and Z.G. were supported by NIH GM131801; and J.F. and D.G. were supported by NIH GM74074.

AUTHOR CONTRIBUTIONS

Z.G. designed the research, performed the research, and analyzed the data; A.Y.T.P. performed the research; A.B. performed the research; Z.B. analyzed the data; K.S. analyzed the data and secured funding; D.G. performed the research; J.F. analyzed the data and secured funding; B.C.F. designed the research, performed the research, analyzed the data, wrote the paper, and secured funding.

DECLARATION OF INTERESTS

The authors declare no competing interests.

STAR★METHODS

Detailed methods are provided in the online version of this paper and include the following:

- KEY RESOURCES TABLE
- EXPERIMENTAL MODEL AND STUDY PARTICIPANT DETAILS
- METHOD DETAILS
  - Cell fractionation for size exclusion chromatography
  - RNA isolation and quantification
  - RNA-seq
  - DNase-seq
  - Histone tail post-translation modification mass spectrometry
  - tU-seq and RNA half-life calculations
  - Chromatin immunoprecipitation assay
  - Anchor-away and GFP-nanobody nuclear-depletion assays
  - TRiC protein purification
  - Nuclear extract preparation
  - *In vitro* transcription assay
  - Template pull-down
  - Purification of TAP-tagged Proteins and CBP-tagged CCT complexes
  - Microscopy
  - Cell viability spot-test
  - Immunoblot figure generation
- QUANTIFICATION AND STATISTICAL ANALYSIS

SUPPLEMENTAL INFORMATION

Supplemental information can be found online at https://doi.org/10.1016/j.molcel.2026.08.015.

Received: August 15, 2024
Revised: April 30, 2026
Accepted: August 13, 2026
Published: September 8, 2026

REFERENCES

1. Gestaut, D., Limatola, A., Joachimiak, L., and Frydman, J. (2019). The ATP-powered gymnastics of TRiC/CCT: an asymmetric protein folding machine with a symmetric origin story. Curr. Opin. Struct. Biol. *55*, 50–58. https://doi.org/10.1016/j.sbi.2019.03.002.
2. Georgopoulos, C.P., Hendrix, R.W., Casjens, S.R., and Kaiser, A.D. (1973). Host participation in bacteriophage lambda head assembly. J. Mol. Biol. *76*, 45–60. https://doi.org/10.1016/0022-2836(73)90080-6.
3. Sternberg, N. (1973). Properties of a mutant of Escherichia coli defective in bacteriophage λ head formation (groE). J. Mol. Biol. *76*, 25–44. https://doi.org/10.1016/0022-2836(73)90079-X.
4. Ewalt, K.L., Hendrick, J.P., Houry, W.A., and Hartl, F.U. (1997). In Vivo Observation of Polypeptide Flux through the Bacterial Chaperonin System. Cell *90*, 491–500. https://doi.org/10.1016/S0092-8674(00)80509-7.
5. Houry, W.A., Frishman, D., Eckerskorn, C., Lottspeich, F., and Hartl, F.U. (1999). Identification of in vivo substrates of the chaperonin GroEL. Nature *402*, 147–154. https://doi.org/10.1038/45977.
6. Yam, A.Y., Xia, Y., Lin, H.-T.J., Burlingame, A., Gerstein, M., and Frydman, J. (2008). Defining the TRiC/CCT interactome links chaperonin function to stabilization of newly made proteins with complex topologies. Nat. Struct. Mol. Biol. *15*, 1255–1262. https://doi.org/10.1038/nsmb.1515.
7. Stein, K.C., Kriel, A., and Frydman, J. (2019). Nascent polypeptide domain topology and elongation rate direct the cotranslational hierarchy of Hsp70 and TRiC/CCT. Mol. Cell *75*, 1117–1130.e5. https://doi.org/10.1016/j.molcel.2019.06.036.
8. Hayer-Hartl, M., Bracher, A., and Hartl, F.U. (2016). The GroEL-GroES Chaperonin Machine, A Nano-Cage for Protein Folding. Trends Biochem. Sci. *41*, 62–76. https://doi.org/10.1016/j.tibs.2015.07.009.
9. Albanèse, V., Yam, A.Y.W., Baughman, J., Parnot, C., and Frydman, J. (2006). Systems analyses reveal two chaperone networks with distinct functions in eukaryotic cells. Cell *124*, 75–88. https://doi.org/10.1016/j.cell.2005.11.039.
10. Dunn, A.Y., Melville, M.W., and Frydman, J. (2001). Review: Cellular Substrates of the Eukaryotic Chaperonin TRiC/CCT. J. Struct. Biol. *135*, 176–184. https://doi.org/10.1006/jsbi.2001.4380.
11. Liu, X., Lin, C.-Y., Lei, M., Yan, S., Zhou, T., and Erikson, R.L. (2005). CCT chaperonin complex is required for the biogenesis of functional Plk1. Mol. Cell. Biol. *25*, 4993–5010. https://doi.org/10.1128/MCB.25.12.4993-5010.2005.
12. Camasses, A., Bogdanova, A., Shevchenko, A., and Zachariae, W. (2003). The CCT chaperonin promotes activation of the anaphase-promoting complex through the generation of functional Cdc20. Mol. Cell *12*, 87–100. https://doi.org/10.1016/s1097-2765(03)00244-2.
13. Plimpton, R.L., Cuéllar, J., Lai, C.W.J., Aoba, T., Makaju, A., Franklin, S., Mathis, A.D., Prince, J.T., Carrascosa, J.L., Valpuesta, J.M., et al. (2015). Structures of the Gβ-CCT and PhLP1-Gβ-CCT complexes reveal a mechanism for G-protein β-subunit folding and Gβγ dimer assembly. Proc. Natl. Acad. Sci. USA *112*, 2413–2418. https://doi.org/10.1073/pnas.1419595112.
14. Balchin, D., Miličić, G., Strauss, M., Hayer-Hartl, M., and Hartl, F.U. (2018). Pathway of actin folding directed by the eukaryotic chaperonin TRiC. Cell *174*, 1507–1521.e16. https://doi.org/10.1016/j.cell.2018.07.006.
15. Feldman, D.E., Thulasiraman, V., Ferreyra, R.G., and Frydman, J. (1999). Formation of the VHL-elongin BC tumor suppressor complex is mediated by the chaperonin TRiC. Mol. Cell *4*, 1051–1061. https://doi.org/10.1016/s1097-2765(00)80233-6.
16. Wells, C.A., Dingus, J., and Hildebrandt, J.D. (2006). Role of the chaperonin CCT/TRiC complex in G protein betagamma-dimer assembly. J. Biol. Chem. *281*, 20221–20232. https://doi.org/10.1074/jbc.M602409200.
17. Seo, S., Baye, L.M., Schulz, N.P., Beck, J.S., Zhang, Q., Slusarski, D.C., and Sheffield, V.C. (2010). BBS6, BBS10, and BBS12 form a complex

with CCT/TRiC family chaperonins and mediate BBSome assembly. Proc. Natl. Acad. Sci. USA *107*, 1488–1493. https://doi.org/10.1073/pnas.0910268107.

18. Antonova, S.V., Haffke, M., Corradini, E., Mikuciunas, M., Low, T.Y., Signor, L., van Es, R.M., Gupta, K., Scheer, E., Vos, H.R., et al. (2018). Chaperonin CCT Checkpoint Function in Basal Transcription Factor TFIID Assembly. Nat. Struct. Mol. Biol. *25*, 1119–1127. https://doi.org/10.1038/s41594-018-0156-z.
19. Brackley, K.I., and Grantham, J. (2011). Interactions between the actin filament capping and severing protein gelsolin and the molecular chaperone CCT: evidence for nonclassical substrate interactions. Cell Stress Chaperones *16*, 173–179. https://doi.org/10.1007/s12192-010-0230-x.
20. Svanström, A., and Grantham, J. (2016). The molecular chaperone CCT modulates the activity of the actin filament severing and capping protein gelsolin in vitro. Cell Stress Chaperones *21*, 55–62. https://doi.org/10.1007/s12192-015-0637-5.
21. Hodeify, R., Nandakumar, M., Own, M., Courjaret, R.J., Graumann, J., Hubrack, S.Z., and Machaca, K. (2018). The CCT chaperonin is a novel regulator of Ca2+ signaling through modulation of Orai1 trafficking. Sci. Adv. *4*, eaau1935. https://doi.org/10.1126/sciadv.aau1935.
22. Stoldt, V., Rademacher, F., Kehren, V., Ernst, J.F., Pearce, D.A., and Sherman, F. (2016). The Cct eukaryotic chaperonin subunits of Saccharomyces cerevisiae and other yeasts. Yeast, 523–529. *12* 2-c.
23. Lewis, V.A., Hynes, G.M., Zheng, D., Saibil, H., and Willison, K. (1992). T-complex polypeptide-1 is a subunit of a heteromeric particle in the eukaryotic cytosol. Nature *358*, 249–252. https://doi.org/10.1038/358249a0.
24. Thulasiraman, V., Yang, C.F., and Frydman, J. (1999). In vivo newly translated polypeptides are sequestered in a protected folding environment. EMBO J. *18*, 85–95. https://doi.org/10.1093/emboj/18.1.85.
25. Willison, K., Lewis, V., Zuckerman, K.S., Cordell, J., Dean, C., Miller, K., Lyon, M.F., and Marsh, M. (1989). The t complex polypeptide 1 (TCP-1) is associated with the cytoplasmic aspect of Golgi membranes. Cell *57*, 621–632. https://doi.org/10.1016/0092-8674(89)90131-1.
26. Horwich, A.L., and Willison, K.R. (1993). Protein folding in the cell, functions of two families of molecular chaperone, hsp 60 and TF55-TCP1. In Molecular Chaperones, R.J. Ellis, R.A. Laskey, and G.H. Lorimer, eds. (Springer Netherlands), pp. 57–70. https://doi.org/10.1007/978-94-011-2108-8_8.
27. Joly, E.C., Tremblay, E., Tanguay, R.M., Wu, Y., and Bibor-Hardy, V. (1994). TRiC-P5, a novel TCP1-related protein, is localized in the cytoplasm and in the nuclear matrix. J. Cell Sci. *107*, 2851–2859. https://doi.org/10.1242/jcs.107.10.2851.
28. Roobol, A., and Carden, M.J. (1999). Subunits of the eukaryotic cytosolic chaperonin CCT do not always behave as components of a uniform hetero-oligomeric particle. Eur. J. Cell Biol. *78*, 21–32. https://doi.org/10.1016/S0171-9335(99)80004-1.
29. Gerner, C., Holzmann, K., Meissner, M., Gotzmann, J., Grimm, R., and Sauermann, G. (1999). Reassembling proteins and chaperones in human nuclear matrix protein fractions. J. Cell. Biochem. *74*, 145–151. https://doi.org/10.1002/(SICI)1097-4644(19990801)74:2<145::AID-JCB1>3.0.CO;2-#.
30. Souès, S., Kann, M.-L., Fouquet, J.-P., and Melki, R. (2003). The cytosolic chaperonin CCT associates to cytoplasmic microtubular structures during mammalian spermiogenesis and to heterochromatin in germline and somatic cells. Exp. Cell Res. *288*, 363–373. https://doi.org/10.1016/S0014-4827(03)00248-9.
31. Ho, Y., Gruhler, A., Heilbut, A., Bader, G.D., Moore, L., Adams, S.-L., Millar, A., Taylor, P., Bennett, K., Boutilier, K., et al. (2002). Systematic identification of protein complexes in Saccharomyces cerevisiae by mass spectrometry. Nature *415*, 180–183. https://doi.org/10.1038/415180a.
32. Shevchenko, A., Schaft, D., Roguev, A., Pijnappel, W.W.M.P., Stewart, A.F., and Shevchenko, A. (2002). Deciphering Protein Complexes and Protein Interaction Networks by Tandem Affinity Purification and Mass Spectrometry, Analytical Perspective. Mol. Cell. Proteomics *1*, 204–212. https://doi.org/10.1074/mcp.M200005-MCP200.
33. Carrozza, M.J., Li, B., Florens, L., Suganuma, T., Swanson, S.K., Lee, K.K., Shia, W.-J., Anderson, S., Yates, J., Washburn, M.P., et al. (2005). Histone H3 Methylation by Set2 Directs Deacetylation of Coding Regions by Rpd3S to Suppress Spurious Intragenic Transcription. Cell *123*, 581–592. https://doi.org/10.1016/j.cell.2005.10.023.
34. Dekker, C., Stirling, P.C., McCormack, E.A., Filmore, H., Paul, A., Brost, R.L., Costanzo, M., Boone, C., Leroux, M.R., and Willison, K.R. (2008). The interaction network of the chaperonin CCT. EMBO J. *27*, 1827–1839. https://doi.org/10.1038/emboj.2008.108.
35. Shevchenko, A., Roguev, A., Schaft, D., Buchanan, L., Habermann, B., Sakalar, C., Thomas, H., Krogan, N.J., Shevchenko, A., and Stewart, A.F. (2008). Chromatin Central: towards the comparative proteome by accurate mapping of the yeast proteomic environment. Genome Biol. *9*, R167. https://doi.org/10.1186/gb-2008-9-11-r167.
36. Guenther, M.G., Yu, J., Kao, G.D., Yen, T.J., and Lazar, M.A. (2002). Assembly of the SMRT–histone deacetylase 3 repression complex requires the TCP-1 ring complex. Genes Dev. *16*, 3130–3135. https://doi.org/10.1101/gad.1037502.
37. Ishihama, A., Ikeuchi, T., and Yura, T. (1976). A novel adenosine triphosphatase isolated from RNA polymerase preparations of Escherichia coli: Copurification and separation. J. Biochem. *79*, 917–925. https://doi.org/10.1093/oxfordjournals.jbchem.a131159.
38. Georgellis, D., Sohlberg, B., Hartl, F.U., and von Gabain, A. (1995). Identification of GroEL as a constituent of an mRNA-protection complex in Escherichia coli. Mol. Microbiol. *16*, 1259–1268. https://doi.org/10.1111/j.1365-2958.1995.tb02347.x.
39. Mukherjee, K., Nagai, H., Shimamoto, N., and Chatterji, D. (1999). GroEL is involved in activation of Escherichia coli RNA polymerase devoid of the ω subunit in vivo. Eur. J. Biochem. *266*, 228–235. https://doi.org/10.1046/j.1432-1327.1999.00848.x.
40. Gestaut, D., Roh, S.H., Ma, B., Pintilie, G., Joachimiak, L.A., Leitner, A., Walzthoeni, T., Aebersold, R., Chiu, W., and Frydman, J. (2019). The Chaperonin TRiC/CCT Associates with Prefoldin through a Conserved Electrostatic Interface Essential for Cellular Proteostasis. Cell *177*, 751–765.e15. https://doi.org/10.1016/j.cell.2019.03.012.
41. Ursic, D., Sedbrook, J.C., Himmel, K.L., and Culbertson, M.R. (1994). The essential yeast Tcp1 protein affects actin and microtubules. Mol. Biol. Cell *5*, 1065–1080. https://doi.org/10.1091/mbc.5.10.1065.
42. Donczew, R., Warfield, L., Pacheco, D., Erijman, A., and Hahn, S. (2020). Two roles for the yeast transcription coactivator SAGA and a set of genes redundantly regulated by TFIID and SAGA. eLife *9*, e50109. https://doi.org/10.7554/eLife.50109.
43. Feng, J., Meyer, C.A., Wang, Q., Liu, J.S., Shirley Liu, X., and Zhang, Y. (2012). GFOLD: a generalized fold change for ranking differentially expressed genes from RNA-seq data. Bioinformatics *28*, 2782–2788. https://doi.org/10.1093/bioinformatics/bts515.
44. Gasch, A.P., Spellman, P.T., Kao, C.M., Carmel-Harel, O., Eisen, M.B., Storz, G., Botstein, D., and Brown, P.O. (2000). Genomic Expression Programs in the Response of Yeast Cells to Environmental Changes. Mol. Biol. Cell *11*, 4241–4257. https://doi.org/10.1091/mbc.11.12.4241.
45. Neil, H., Malabat, C., d'Aubenton-Carafa, Y., Xu, Z., Steinmetz, L.M., and Jacquier, A. (2009). Widespread bidirectional promoters are the major source of cryptic transcripts in yeast. Nature *457*, 1038–1042. https://doi.org/10.1038/nature07747.
46. Xu, Z., Wei, W., Gagneur, J., Perocchi, F., Clauder-Münster, S., Camblong, J., Guffanti, E., Stutz, F., Huber, W., and Steinmetz, L.M. (2009). Bidirectional promoters generate pervasive transcription in yeast. Nature *457*, 1033–1037. https://doi.org/10.1038/nature07728.

47. van Dijk, E.L., Chen, C.L., d'Aubenton-Carafa, Y., Gourvennec, S., Kwapisz, M., Roche, V., Bertrand, C., Silvain, M., Legoix-Né, P., Loeillet, S., et al. (2011). XUTs are a class of Xrn1-sensitive antisense regulatory non-coding RNA in yeast. Nature *475*, 114–117. https://doi.org/10.1038/nature10118.

48. Schulz, D., Schwalb, B., Kiesel, A., Baejen, C., Torkler, P., Gagneur, J., Soeding, J., and Cramer, P. (2013). Transcriptome Surveillance by Selective Termination of Noncoding RNA Synthesis. Cell *155*, 1075–1087. https://doi.org/10.1016/j.cell.2013.10.024.

49. Singh, P., Chaudhuri, A., Banerjea, M., Marathe, N., and Das, B. (2021). Nrd1p identifies aberrant and natural exosomal target messages during the nuclear mRNA surveillance in Saccharomyces cerevisiae. Nucleic Acids Res. *49*, 11512–11536. https://doi.org/10.1093/nar/gkab930.

50. Gvozdenov, Z., Kolhe, J., and Freeman, B.C. (2019). The Nuclear and DNA-Associated Molecular Chaperone Network. Cold Spring Harb. Perspect. Biol. *11*, a034009. https://doi.org/10.1101/cshperspect.a034009.

51. Pesavento, J.J., Mizzen, C.A., and Kelleher, N.L. (2006). Quantitative Analysis of Modified Proteins and Their Positional Isomers by Tandem Mass Spectrometry: Human Histone H4. Anal. Chem. *78*, 4271–4280. https://doi.org/10.1021/ac0600050.

52. Pokholok, D.K., Harbison, C.T., Levine, S., Cole, M., Hannett, N.M., Lee, T.I., Bell, G.W., Walker, K., Rolfe, P.A., Herbolsheimer, E., et al. (2005). Genome-wide Map of Nucleosome Acetylation and Methylation in Yeast. Cell *122*, 517–527. https://doi.org/10.1016/j.cell.2005.06.026.

53. Nguyen, A.T., and Zhang, Y. (2011). The diverse functions of Dot1 and H3K79 methylation. Genes Dev. *25*, 1345–1358. https://doi.org/10.1101/gad.2057811.

54. Xue, Y., Van, C., Pradhan, S.K., Su, T., Gehrke, J., Kuryan, B.G., Kitada, T., Vashisht, A., Tran, N., Wohlschlegel, J., et al. (2015). The Ino80 complex prevents invasion of euchromatin into silent chromatin. Genes Dev. *29*, 350–355. https://doi.org/10.1101/gad.256255.114.

55. Li, B., Pattenden, S.G., Lee, D., Gutiérrez, J., Chen, J., Seidel, C., Gerton, J., and Workman, J.L. (2005). Preferential occupancy of histone variant H2AZ at inactive promoters influences local histone modifications and chromatin remodeling. Proc. Natl. Acad. Sci. USA *102*, 18385–18390. https://doi.org/10.1073/pnas.0507975102.

56. Zhang, H., Roberts, D.N., and Cairns, B.R. (2005). Genome-Wide Dynamics of Htz1, a Histone H2A Variant that Poises Repressed/Basal Promoters for Activation through Histone Loss. Cell *123*, 219–231. https://doi.org/10.1016/j.cell.2005.08.036.

57. Ng, H.H., Feng, Q., Wang, H., Erdjument-Bromage, H., Tempst, P., Zhang, Y., and Struhl, K. (2002). Lysine methylation within the globular domain of histone H3 by Dot1 is important for telomeric silencing and Sir protein association. Genes Dev. *16*, 1518–1527. https://doi.org/10.1101/gad.1001502.

58. Haruki, H., Nishikawa, J., and Laemmli, U.K. (2008). The Anchor-Away Technique: Rapid, Conditional Establishment of Yeast Mutant Phenotypes. Mol. Cell *31*, 925–932. https://doi.org/10.1016/j.molcel.2008.07.020.

59. Zelin, E., Zhang, Y., Toogun, O.A., Zhong, S., and Freeman, B.C. (2012). The p23 Molecular Chaperone and GCN5 Acetylase Jointly Modulate Protein-DNA Dynamics and Open Chromatin Status. Mol. Cell *48*, 459–470. https://doi.org/10.1016/j.molcel.2012.08.026.

60. Echtenkamp, F.J., Gvozdenov, Z., Adkins, N.L., Zhang, Y., Lynch-Day, M., Watanabe, S., Peterson, C.L., and Freeman, B.C. (2016). Hsp90 and p23 Molecular Chaperones Control Chromatin Architecture by Maintaining the Functional Pool of the RSC Chromatin Remodeler. Mol. Cell *64*, 888–899. https://doi.org/10.1016/j.molcel.2016.09.040.

61. Gvozdenov, Z., Bendix, L.D., Kolhe, J., and Freeman, B.C. (2019). The Hsp90 Molecular Chaperone Regulates the Transcription Factor Network Controlling Chromatin Accessibility. J. Mol. Biol. *431*, 4993–5003. https://doi.org/10.1016/j.jmb.2019.09.007.

62. Hesselberth, J.R., Chen, X., Zhang, Z., Sabo, P.J., Sandstrom, R., Reynolds, A.P., Thurman, R.E., Neph, S., Kuehn, M.S., Noble, W.S., et al. (2009). Global mapping of protein-DNA interactions in vivo by digital genomic footprinting. Nat. Methods *6*, 283–289. https://doi.org/10.1038/nmeth.1313.

63. John, S., Sabo, P.J., Thurman, R.E., Sung, M.H., Biddie, S.C., Johnson, T.A., Hager, G.L., and Stamatoyannopoulos, J.A. (2011). Chromatin accessibility pre-determines glucocorticoid receptor binding patterns. Nat. Genet. *43*, 264–268. https://doi.org/10.1038/ng.759.

64. Jensen, T.H., Jacquier, A., and Libri, D. (2013). Dealing with Pervasive Transcription. Mol. Cell *52*, 473–484. https://doi.org/10.1016/j.molcel.2013.10.032.

65. Barrass, J.D., Reid, J.E.A., Huang, Y., Hector, R.D., Sanguinetti, G., Beggs, J.D., and Granneman, S. (2015). Transcriptome-wide RNA processing kinetics revealed using extremely short 4tU labeling. Genome Biol. *16*, 282. https://doi.org/10.1186/s13059-015-0848-1.

66. Schwalb, B., Michel, M., Zacher, B., Frühauf, K., Demel, C., Tresch, A., Gagneur, J., and Cramer, P. (2016). TT-seq maps the human transient transcriptome. Science *352*, 1225–1228. https://doi.org/10.1126/science.aad9841.

67. Blumberg, A., Zhao, Y., Huang, Y.-F., Dukler, N., Rice, E.J., Chivu, A.G., Krumholz, K., Danko, C.G., and Siepel, A. (2021). Characterizing RNA stability genome-wide through combined analysis of PRO-seq and RNA-seq data. BMC Biol. *19*, 30. https://doi.org/10.1186/s12915-021-00949-x.

68. Xing, H., Rosenkranz, R.R.E., Rodriguez-Aliaga, P., Lee, T.-T., Majtner, T., Böhm, S., Turoňová, B., Frydman, J., and Beck, M. (2025). In situ analysis reveals the TRiC duty cycle and PDCD5 as an open-state cofactor. Nature *637*, 983–990. https://doi.org/10.1038/s41586-024-08321-z.

69. Wang, A., Kolhe, J.A., Gioacchini, N., Baade, I., Brieher, W.M., Peterson, C.L., and Freeman, B.C. (2020). Mechanism of Long-Range Chromosome Motion Triggered by Gene Activation. Dev. Cell *52*, 309–320.e5. https://doi.org/10.1016/j.devcel.2019.12.007.

70. Miklos, D., Caplan, S., Mertens, D., Hynes, G., Pitluk, Z., Kashi, Y., Harrison-Lavoie, K., Stevenson, S., Brown, C., and Barrell, B. (1994). Primary structure and function of a second essential member of the heterooligomeric TCP1 chaperonin complex of yeast, TCP1 beta. Proc. Natl. Acad. Sci. USA *91*, 2743–2747. https://doi.org/10.1073/pnas.91.7.2743.

71. Pappenberger, G., McCormack, E.A., and Willison, K.R. (2006). Quantitative Actin Folding Reactions using Yeast CCT Purified via an Internal Tag in the CCT3/γ Subunit. J. Mol. Biol. *360*, 484–496. https://doi.org/10.1016/j.jmb.2006.05.003.

72. Schulte, J., and Littleton, J.T. (2011). The biological function of the Huntingtin protein and its relevance to Huntington's Disease pathology. Curr. Trends Neurol. *5*, 65–78.

73. Duyao, M., Ambrose, C., Myers, R., Novelletto, A., Persichetti, F., Frontali, M., Folstein, S., Ross, C., Franz, M., and Abbott, M. (1993). Trinucleotide repeat length instability and age of onset in Huntington's disease. Nat. Genet. *4*, 387–392. https://doi.org/10.1038/ng0893-387.

74. Chan, E.Y.W., Luthi-Carter, R., Strand, A., Solano, S.M., Hanson, S.A., DeJohn, M.M., Kooperberg, C., Chase, K.O., DiFiglia, M., Young, A.B., et al. (2002). Increased huntingtin protein length reduces the number of polyglutamine-induced gene expression changes in mouse models of Huntington's disease. Hum. Mol. Genet. *11*, 1939–1951. https://doi.org/10.1093/hmg/11.17.1939.

75. Soares, T.R., Reis, S.D., Pinho, B.R., Duchen, M.R., and Oliveira, J.M.A. (2019). Targeting the proteostasis network in Huntington's disease. Ageing Res. Rev. *49*, 92–103. https://doi.org/10.1016/j.arr.2018.11.006.

76. Makrantoni, V., Dennison, P., Stark, M.J.R., and Coote, P.J. (2007). A novel role for the yeast protein kinase Dbf2p in vacuolar H+-ATPase

function and sorbic acid stress tolerance. Microbiology (Reading) *153*, 4016–4026. https://doi.org/10.1099/mic.0.2007/010298-0.

77. Jayaraj, G.G., Hipp, M.S., and Hartl, F.U. (2020). Functional Modules of the Proteostasis Network. Cold Spring Harb.. Perspect. Biol. *12*, a033951. https://doi.org/10.1101/cshperspect.a033951.
78. DeZwaan, D.C., and Freeman, B.C. (2008). HSP90: the Rosetta Stone for cellular protein dynamics? Cell Cycle *7*, 1006–1012. https://doi.org/10.4161/cc.7.8.5723.
79. Morales-Polanco, F., Lee, J.H., Barbosa, N.M., and Frydman, J. (2022). Cotranslational Mechanisms of Protein Biogenesis and Complex Assembly in Eukaryotes. Annu. Rev. Biomed. Data Sci. *5*, 67–94. https://doi.org/10.1146/annurev-biodatasci-121721-095858.
80. Rüßmann, F., Stemp, M.J., Mönkemeyer, L., Etchells, S.A., Bracher, A., and Hartl, F.U. (2012). Folding of large multidomain proteins by partial encapsulation in the chaperonin TRiC/CCT. Proc. Natl. Acad. Sci. USA *109*, 21208–21215. https://doi.org/10.1073/pnas.1218836109.
81. Ghozlan, H., Cox, A., Nierenberg, D., King, S., and Khaled, A.R. (2022). The TRiCky Business of Protein Folding in Health and Disease. Front. Cell Dev. Biol. *10*, 906530. https://doi.org/10.3389/fcell.2022.906530.
82. Anastasiadou, E., Jacob, L.S., and Slack, F.J. (2018). Non-coding RNA networks in cancer. Nat. Rev. Cancer *18*, 5–18. https://doi.org/10.1038/nrc.2017.99.
83. Morgan, M., Shiekhattar, R., Shilatifard, A., and Lauberth, S.M. (2022). It's a DoG-eat-DoG world—altered transcriptional mechanisms drive downstream-of-gene (DoG) transcript production. Mol. Cell *82*, 1981–1991. https://doi.org/10.1016/j.molcel.2022.04.008.
84. Abe, K., Maunze, B., Lopez, P.-A., Xu, J., Muhammad, N., Yang, G.-Y., Katz, D., Liu, Y., and Lauberth, S.M. (2024). Downstream-of-gene (DoG) transcripts contribute to an imbalance in the cancer cell transcriptome. Sci. Adv. *10*, eadh9613. https://doi.org/10.1126/sciadv.adh9613.
85. Rutkowski, A.J., Erhard, F., L'Hernault, A., Bonfert, T., Schilhabel, M., Crump, C., Rosenstiel, P., Efstathiou, S., Zimmer, R., Friedel, C.C., et al. (2015). Widespread disruption of host transcription termination in HSV-1 infection. Nat. Commun. *6*, 7126. https://doi.org/10.1038/ncomms8126.
86. Vilborg, A., Passarelli, M.C., Yario, T.A., Tycowski, K.T., and Steitz, J.A. (2015). Widespread Inducible Transcription Downstream of Human Genes. Mol. Cell *59*, 449–461. https://doi.org/10.1016/j.molcel.2015.06.016.
87. Vilborg, A., Sabath, N., Wiesel, Y., Nathans, J., Levy-Adam, F., Yario, T.A., Steitz, J.A., and Shalgi, R. (2017). Comparative analysis reveals genomic features of stress-induced transcriptional readthrough. Proc. Natl. Acad. Sci. USA *114*, E8362–E8371. https://doi.org/10.1073/pnas.1711120114.
88. Rosa-Mercado, N.A., Zimmer, J.T., Apostolidi, M., Rinehart, J., Simon, M.D., and Steitz, J.A. (2021). Hyperosmotic stress alters the RNA Polymerase II interactome and induces readthrough transcription despite widespread transcriptional repression. Mol. Cell *81*, 502–513.e4. https://doi.org/10.1016/j.molcel.2020.12.002.
89. Wei, W., Pelechano, V., Järvelin, A.I., and Steinmetz, L.M. (2011). Functional consequences of bidirectional promoters. Trends Genet. *27*, 267–276. https://doi.org/10.1016/j.tig.2011.04.002.
90. Wight, M., and Werner, A. (2013). The functions of natural antisense transcripts. Essays Biochem. *54*, 91–101. https://doi.org/10.1042/bse0540091.
91. Dave, P., Roth, G., Griesbach, E., Mateju, D., Hochstoeger, T., and Chao, J.A. (2023). Single-molecule imaging reveals translation-dependent destabilization of mRNAs. Mol. Cell *83*, 589–606.e6. https://doi.org/10.1016/j.molcel.2023.01.013.
92. Gvozdenov, Z., Barcutean, Z., and Struhl, K. (2023). Functional analysis of a random-sequence chromosome reveals a high level and the molecular nature of transcriptional noise in yeast cells. Mol. Cell *83*, 1786–1797.e5. https://doi.org/10.1016/j.molcel.2023.04.010.
93. Longtine, M.S., McKenzie, A., Demarini, D.J., Shah, N.G., Wach, A., Brachat, A., Philippsen, P., and Pringle, J.R. (1998). Additional modules for versatile and economical PCR-based gene deletion and modification in Saccharomyces cerevisiae. Yeast *14*, 953–961. https://doi.org/10.1002/(SICI)1097-0061(199807)14,10<953,AID-YEA293>3.0.CO;2-U.
94. Kubota, T., Stead, D.A., Hiraga, S., Ten Have, S., and Donaldson, A.D. (2012). Quantitative proteomic analysis of yeast DNA replication proteins. Methods *57*, 196–202. https://doi.org/10.1016/j.ymeth.2012.03.012.
95. Collart, M.A., and Oliviero, S. (2001). Preparation of Yeast RNA. Curr. Protoc. Mol. Biol. https://doi.org/10.1002/0471142727.mb1312s23.
96. Dobin, A., Davis, C.A., Schlesinger, F., Drenkow, J., Zaleski, C., Jha, S., Batut, P., Chaisson, M., and Gingeras, T.R. (2013). STAR: ultrafast universal RNA-seq aligner. Bioinformatics *29*, 15–21. https://doi.org/10.1093/bioinformatics/bts635.
97. Piper, J., Elze, M.C., Cauchy, P., Cockerill, P.N., Bonifer, C., and Ott, S.W. (2013). Wellington: A novel method for the accurate identification of digital genomic footprints from DNase-seq data. Nucleic Acids Res. *41*, e201. https://doi.org/10.1093/nar/gkt850.
98. Sung, M.-H., Guertin, M.J., Baek, S., and Hager, G.L. (2014). DNase Footprint Signatures are Dictated by Factor Dynamics and DNA Sequence. Mol. Cell *56*, 275–285. https://doi.org/10.1016/j.molcel.2014.08.016.
99. Garcia, B.A., Mollah, S., Ueberheide, B.M., Busby, S.A., Muratore, T.L., Shabanowitz, J., and Hunt, D.F. (2007). Chemical derivatization of histones for facilitated analysis by mass spectrometry. Nat. Protoc. *2*, 933–938. https://doi.org/10.1038/nprot.2007.106.
100. Kuras, L., and Struhl, K. (1999). Binding of TBP to promoters in vivo is stimulated by activators and requires Pol II holoenzyme. Nature *399*, 609–613. https://doi.org/10.1038/21239.
101. Fan, X., Geisberg, J.V., Wong, K.H., and Jin, Y. (2011). Conditional Depletion of Nuclear Proteins by the Anchor Away System. Curr. Protoc. Mol. Biol. https://doi.org/10.1002/0471142727.mb1310bs93.
102. Solís, E.J., Pandey, J.P., Zheng, X., Jin, D.X., Gupta, P.B., Airoldi, E.M., Pincus, D., and Denic, V. (2016). Defining the essential function of yeast Hsf1 reveals a compact transcriptional program for maintaining eukaryotic proteostasis. Mol. Cell *63*, 60–71. https://doi.org/10.1016/j.molcel.2016.05.014.
103. Reeves, W.M., and Hahn, S. (2003). Activator-Independent Functions of the Yeast Mediator Sin4 Complex in Preinitiation Complex Formation and Transcription Reinitiation. Mol. Cell. Biol. *23*, 349–358. https://doi.org/10.1128/MCB.23.1.349-358.2003.
104. Freeman, B.C., and Yamamoto, K.R. (2002). Disassembly of Transcriptional Regulatory Complexes by Molecular Chaperones. Science *296*, 2232–2235. https://doi.org/10.1126/science.1073051.
105. Rines, D.R., Thomann, D., Dorn, J.F., Goodwin, P., and Sorger, P.K. (2011). Live Cell Imaging of Yeast. Cold Spring Harb. Protoc. *2011*. https://doi.org/10.1101/pdb.top065482.

STAR★METHODS

KEY RESOURCES TABLE

REAGENT or RESOURCE	SOURCE	IDENTIFIER
Antibodies		
Anti-TAP	ThermoFisher	Cat# CAB1001; RRID: AB_10709700
Anti-GFP	Santa Cruz	Cat# sc-8334; RRID: AB_641123
Anti-Rpb1	Santa Cruz	Cat# sc-47701; RRID: AB_677353
Anti-Pgk1	Abcam	Cat# ab113687; RRID: AB_2756444
Anti-CCT1/3/6	J. Frydman	N/A
Anti-Actin	Abcam	Cat# AB170325; RRID: AB_2893492
Anti-Tubulin	Developmental Studies Hybridoma Bank	Cat# DSHB 4A1; RRID: AB_2732839
Anti-Sba1	Homemade	N/A
IgG Sepharose	GE Healthcare	Cat# 17-0969-01; RRID: SCR_018374
Calmodulin Affinity Resin	Agilent Technologies	Cat# 214303-52
Anti-GFP agarose beads	Santa Cruz	Cat# sc-9996; RRID: AB_627695
Bacterial and virus strains		
Rosetta(DE3)	Novagen	Cat# 70954-3
Chemicals, peptides, and recombinant proteins		
Yeast nitrogen base without amino acids	DIFCO	Cat# 291940
D-(+)-Glucose	ThermoFisher	Cat# D16-1
Yeast amino acid dropout mix without histidine, leucine, tryptophan, and uracil	Millipore (Merck)	Cat# Y2001
L-Histidine	ThermoFisher	Cat# 166151000
L-Tryptophan	ThermoFisher	Cat# A10230-22
L-Leucine	ThermoFisher	Cat# A12311-22
L-Uracil	ThermoFisher	Cat# 157301000
LB Broth Miller	DIFCO	Cat# 244520
Rapamycin	GoldBio	Cat# R-101
Galactose	Fisher Scientific	Cat# AC150611000
Phenol	Sigma Aldrich	CAS# 108-95-2
Chloroform	Sigma Aldrich	CAS# 67-66-3
Ficoll® 400	Sigma Aldrich	CAS# 26873-85-8
4-thiouracil	Sigma Aldrich	CAS# 591-28-6
SYPRO Ruby Protein Gel Stain	ThermoFisher	Cat#S12000
BamHI	New England BioLabs	Cat# R3136L
BspEI	New England BioLabs	Cat# R0540L
SalI	New England BioLabs	Cat# R0138L
XhoI	New England BioLabs	Cat# R0146L
Critical commercial assays		
Pierce BCA Assay Kit	Fisher Scientific	Cat# PI23223
Power SYBR Green RNA-to-CT 1-Step kit	Applied Biosystems	Cat# 4388869
In-Fusion Snap Assembly kit	Takara Bio	Cat# 638946
Q5 Site-Directed Mutagenesis Kit	New England BioLabs	Cat# E0554S
Deposited data		
Imaging data	Mendeley Data	http://www.doi.org/10.17632/z9pd8p875f.2

(*Continued on next page*)

Continued

REAGENT or RESOURCE	SOURCE	IDENTIFIER
Immunoblot data	Mendeley Data	http://www.doi.org/10.17632/z9pd8p875f.2; GenBank: GSE274453, GSE274454, GSE274455875f.2
RNA-Seq	This study	GSE274453
DNaseI-Seq	This study	GSE274454
4tU-Seq	This study	GSE274455
Experimental models: Organisms/strains		
W303 *cct6Δ*::HIS3 pAB-CCT6-CBP::LEU2 (CCT6-CBP)	This study	N/A
BY4741 *cct2Δ*::KanMX pAB-CCT2-GFP::LEU2 (CCT2-GFP)	Gestaut et al.[40]	N/A
BY4741 *cct6Δ*::HIS3 pAB-CCT6-GFP::LEU2 (CCT6-GFP)	Gestaut et al.[40]	N/A
BY4741 *cct6Δ*::HIS3 pAB-CCT6-GFP::LEU2 Rpb3-mCh::hphMX (CCT6-GFP Rpb3-mCh)	This study	N/A
CCT1 WT	J. Frydman	N/A
cct1-2	J. Frydman	N/A
CCT1 WT Rpb1-TAP:: HIS3	This study	N/A
cct1-2 Rpb1-TAP:: HIS3	This study	N/A
CCT1 WT H2A.Z-TAP:: HIS3	This study	N/A
cct1-2 H2A.Z-TAP:: HIS3	This study	N/A
CCT1 WT *htz1Δ*:: KanMX	This study	N/A
cct1-2 htz1Δ:: KanMX	This study	N/A
CCT1 WT H2A.Z-FRB:: KanMX	This study	N/A
BY4741 CCT6-FRB::KanMX	This study	N/A
CCT4 WT	J. Frydman	N/A
cct4-1	J. Frydman	N/A
Oligonucleotides		
VAS1 GENE F (CGCTTTTATCAGTCCCAGGC)	Integrated DNA technologies (IDT)	N/A
VAS1 GENE R (GTCAACAGCTTCCTTGTCGG)	Integrated DNA technologies (IDT)	N/A
VAS1 IT F (AGTCATGCTACCTCTGAACGT)	Integrated DNA technologies (IDT)	N/A
VAS1 IT R (AACGATGACAGCCAGTGGTA)	Integrated DNA technologies (IDT)	N/A
DRN1 GENE F (GAGCCTTTCCAGTGGGAAAGAG)	Integrated DNA technologies (IDT)	N/A
DRN1 GENE R (CGGGTTAGCTATCAAGTTGGGC)	Integrated DNA technologies (IDT)	N/A
DRN1 IT F (CTCAGTTCACGGTAACGGTCC)	Integrated DNA technologies (IDT)	N/A
DRN1 IT R (CCTTCTAAGAGAGCTACCTTGCG)	Integrated DNA technologies (IDT)	N/A
DBF2 GENE F (GGCTATGGAATTTGTACCAGGC)	Integrated DNA technologies (IDT)	N/A
DBF2 GENE R (GCTGGAAATTCCAGGTCCTTG)	Integrated DNA technologies (IDT)	N/A
DBF2 IT F (CAAACACCACACGCTGCAACC)	Integrated DNA technologies (IDT)	N/A
DBF2 IT R (CTTGGACGAATTGCCTCCTTG)	Integrated DNA technologies (IDT)	N/A
PRP31 GENE F (CGAAATCATCCCCCTCATCAAG)	Integrated DNA technologies (IDT)	N/A
PRP31 GENE R (CCTCGTTTTGATGTCCAATGGC)	Integrated DNA technologies (IDT)	N/A
PRP31 IT F (GCAGCCGGCAGTTTACATAAAG)	Integrated DNA technologies (IDT)	N/A
PRP31 IT R (GCTTTATTCTGAGCGTCGCCAC)	Integrated DNA technologies (IDT)	N/A

(*Continued on next page*)

Continued		
REAGENT or RESOURCE	SOURCE	IDENTIFIER
SSA1_qPCR_F (GGTGACACCCATTTGGGTGGTG)	Integrated DNA technologies (IDT)	N/A
SSA1_qPCR_R (CGGAAGTTTGAGCGGAGGAAGAC)	Integrated DNA technologies (IDT)	N/A
ACT1_qPCR_F (AACGATGACAGCCAGTGGTA)	Integrated DNA technologies (IDT)	N/A
ACT1_qPCR_R (GAAGGCTGGAACGTTGAAAG)	Integrated DNA technologies (IDT)	N/A
Recombinant DNA		
pAB-CCT2-GFP	Gestaut et al.[40]	N/A
pAB-CCT6-GFP	Gestaut et al.[40]	N/A
pAB-CCT6-CBP	Gestaut et al.[40]	N/A
p406-GAL1-3xNES-GFP nanobody-CASQ	This study	N/A
p406-GAL1-3xNES-GFP nanobody-CASQ-GPD-mChER05	This study	N/A
pESC-URA3 HttQ104-GFP	J. Frydman	N/A
Software and algorithms		
Interval Identifier	Gvozdenov et al.[92]	https://zenodo.org/records/7804010

EXPERIMENTAL MODEL AND STUDY PARTICIPANT DETAILS

Saccharomyces cerevisiae cultures were grown in complete (YPD) or minimal media supplemented with the required amino acids at 30°C unless otherwise noted. TAP-tagged variants were produced by standard recombinant methods by introducing the fusion tag into either parental (WT) or *cct1-2* yeast.[93] Yeast expressing the CCT subunits Cct2 and Cct6 as GFP fusions were obtained from Judith Frydman (Stanford University).[40]

METHOD DETAILS

Cell fractionation for size exclusion chromatography

Cell fractionation was performed using cells treated with 0.1% sodium azide to halt nuclear transport before spheroplasting.[94] An aliquot was removed before lysis by Dounce homogenization representing the whole cell extract. Upon centrifugation, 5% of total cell amount was taken from the supernatant (Cytoplasmic fraction) which was concentrated using TCA (10%) precipitation. The pellet was resuspended in 8% PVP with 0.025% Triton X-100 in 20 mM potassium phosphate buffer pH 6.5, 1 mM MgCl2, 1 mM DTT and protease inhibitors and incubated on ice for 10 min. Nuclei were obtained by centrifugation at 10,000xg for 5 min. Cell fractionation was visualized via immunoblotting using rabbit anti-GFP (sc-8334), mouse anti-PGK1 (Invitrogen ab113687) and mouse anti-Pol II (CTD) (Santa Cruz sc-47701). Whole cell extract and nuclear fractions also were resolved by size exclusion chromatography using a Superdex-200 column (Cytiva). After passage of the void volume, 1 mL fractions were collected, precipitated with TCA (10% final), and the samples were analyzed by immunoblot using a rabbit anti-GFP (sc-8334).

RNA isolation and quantification

Total RNA was extracted using hot phenol extraction.[95] RT-qPCR reactions were performed with the Power SYBR Green RNA-to-C_T 1-Step Kit according to the manufacturer's instructions (Applied Biosystems).

RNA-seq

Total RNA was isolated from WT or *cct1-2* yeast using Yeast RiboPure RNA purification kit (Ambion) from cells grown to log phase at 30°C and then shifted to 37°C for 4 h. The libraries were prepared using TruSeq Stranded mRNA kit (Illumina) according to the manufacturer's instructions, the samples were sequenced on an Illumina HiSeq2000 and processed with Casava 1.8.2. The trimmed reads were aligned to the sacCer3 reference genome (UCSC) with STAR and differences in gene expression were determined with GFold.[43,96]

DNase-seq

The DNase-Seq were performed using WT or *cct1-2* yeast pellets collected from log rhythmically growing cells at 30°C that were shifted to 37°C for 4 h. The pellets were washed with 1 M sorbitol, 50 mM K-phosphate pH 6.5, 0.018% β-mercaptoethanol then

treated with zymolyase 20T until 50%–60% spheroplast formation was achieved. Spheroplasts were dounced in 18% Ficoll 400, 20 mM K-phosphate pH 6.8, 1 mM $CaCl_2$, 0.5 mM EDTA-NaOH pH 8, 3 mM DTT, 1 mM PMSF with protease inhibitors. Crude nuclei were collected at 13,000 rpm for 30 min and were digested with 2–5 U/ml of DNase I for 5 min at RT. The reaction was terminated by adding 500 μl Stop buffer (50 mM Tris-HCl pH 8, 100 mM NaCl, 0.1% SDS, 100 mM EDTA-NaOH pH 8, 1 mM spermidine, 0.3 mM spermine, 10 μg/μl ribonuclease A). 20 μg proteinase K was added to each sample and incubated overnight at 55°C. The DHS fragments were isopropanol precipitated and reconstituted in 25 mM Tris pH 9. DNA was isolated, resolved on a 1% agarose gel, the DNAs in the size range of 100–650 bp were excised, DNA was isolated using a QIAprep Spin MiniPrep columns (QIAGEN), and sequenced on an Illumina HiSeq2000. Sequence reads were aligned to the sacCer3 reference genome (UCSC) using Bowtie (0.12.8), DNaseI hypersensitive sites were identified using hotspot (v4) and DNA footprints were identified using JASPAR.[59,61,62,97,98]

Histone tail post-translation modification mass spectrometry

Total histones were isolated from WT or *cct1-2* yeast grown to log phase at 30°C and shifted to 37°C for 4 h using acid histone extraction.[99] Nuclei were prepared from the collected cells using Nuclei Isolation Buffer (15 mM Tris (pH 7.5), 60 mM KCl, 15 mM NaCl, 5 mM $MgCl_2$, 1 mM $CaCl_2$, 250 mM sucrose, 1 mM DTT, 2 mM sodium vanadate, 1x protease inhibitor mix, 10 mM sodium butyrate), as described. Following nuclei lysis, the extracts were precipitated with trichloroacetic acid, the pellets were resuspended in acetone supplemented with 0.1% HCl, and the isolated histones were sent for mass spectrometry analysis (IMSERC, Northwestern University).

tU-seq and RNA half-life calculations

The 4tU-Seq and RNA half-life calculations were performed using a 4tU-Seq protocol.[92] Briefly, WT or *cct1-2* yeast were grown to log phase at 30°C, shifted to 37°C for 4 h, treated with either 4-thiouracil (4tU, Sigma Aldrich; 5 mM final) or DMSO for 5 min. Spike-in control cells, untreated *S. cerevisiae* or *K. lactis* cells treated with 4tU for 5 min, were added to the sample before RNA extraction. Following poly(A) RNA enrichment, fragmentation, and repair, the RNA was biotinylated with activated disulfide methane thiosulfonate (MTS) biotin (Biotium Biotin-XX MTSEA). Biotinylated RNA was collected using glycogen blocked MyOne Streptavidin C1 Dynabeads (Invitrogen). Following sequencing, the duplicate reads were removed, and spike-in normalized nucleotide coverages were used to subtract background from the 4tU samples to obtain active transcription measurements. RNA half-life calculations were determined using the combined RNA-Seq and 4tU-Seq values.[65,67] Briefly, the unitless constant of RNA half-life was estimated from the number of transcripts (RNA-Seq) divided by the production of new mRNA (4tU-Seq), with RNA-Seq and 4tU-Seq expressed as transcripts per million (TPMs).

Chromatin immunoprecipitation assay

Chromatin immunoprecipitations were performed with WT or *cct1-2* yeast expressing the protein of interest as a TAP-tagged fusion were grown to log phase at 30°C, shifted to 37°C for 4 h and fixed with 1% formaldehyde for 15 min at RT followed by quenching with 2.5 M glycine for 15 min.[60,100] Cells were lysed in FA lysis buffer (50 mM HEPES pH 7.5, 150 mM NaCl, 1 mM EDTA pH 8, 1% TritonX-100, 0.1 % Na-deoxycholate, 0.1% SDS and 2 mM PMSF) by bead beating for 37 min. Fixed chromatin was collected and sheared by sonication to ~500 bp and incubated with IgG Sepharose beads (GE Healthcare) for 2 h at 22°C. Beads were then washed with FA lysis buffer with 500 mM NaCl, ChIP Wash buffer (10 mM Tris-HCl pH 8, 250 mM LiCl, 1 mM EDTA pH 8, 0.5% NP-40, 0.5% Na-deoxycholate) and DNA was eluted with ChIP Elution Buffer (50 mM Tris-HCl pH 8, 10 mM EDTA pH 8, 1% SDS) and incubated with 20 μl of 20 mg/ml proteinase K at 65 °C overnight. DNA was isolated using QIAprep Spin Miniprep columns (Qiagen) and analyzed by qPCR using primers as indicated. qPCR values were normalized relative to the control site *ACT1*.

Anchor-away and GFP-nanobody nuclear-depletion assays

To conditionally deplete yeast nuclei of the H2A.Z histone, we used a standard anchor away tactic.[58,101] Briefly, the endogenous H2A.Z encoding gene (*HTZ1*) was engineered to express the protein as a carboxyl-terminal FRB fusion in a yeast background of *fpr1*Δ*tor1-1* (VDY1874).[102] Rapamycin (1 μg/ml final) addition was used to trigger nuclear depletion or with ethanol addition as a control. To conditionally deplete yeast nuclei of TRiC, we exploited the strains expressing the Cct2 or Cct6 subunits as GFP fusions along with the inducible expression (GAL1p) of a GFP nanobody with nuclear export signal (NES). Transformants were grown in selective minimal media supplemented with raffinose (2%) to early log phase, galactose was added (2% final), and GFP signal was monitored by immunofluorescence.

TRiC protein purification

The TRiC complex was purified as previously High Five insect cells expressing His-tagged TRiC with GFP-Cct1 were collected and lysed by Dounce homogenization.[40] The TRiC complex was captured by affinity purification using nickel resin. The TRiC complex was sequentially passaged over a heparin column, Mono Q ion exchange column, and Superose 6 size exclusion column. TRiC containing fractions were pooled, concentrated, and snap-frozen in liquid nitrogen.

Nuclear extract preparation

Functional nuclear extracts were prepared as described on the Hahn laboratory website (https://research.fredhutch.org/hahn/en/methods.html), with modifications.[103] Briefly, parental or *cct1-2* yeast grown at 37°C for 4 h were collected for spheroplasting and lysis by Dounce homogenization. The crude nuclei were lysed using 0.5 M ammonium sulfate and clarified using a SW55Ti rotor at 34100 rpm for 50 min at 4°C. Extracts were then clarified using a SW55Ti rotor at 12200 rpm for 15 min at 4 °C. The resulting pellet was resuspended and dialyzed with 3 changes of Buffer C (500 mL) supplemented with 75 mM ammonium sulfate for a total of 4.5 h. Protein concentration of the nuclear extracts were determined using the BCA assay and stored in aliquots for in vitro transcription.

In vitro transcription assay

The *VAS1* (+100 to -50) DNA template for the in vitro transcription reactions was amplified from genomic DNA isolated from wild type yeast using an upstream primer with a biotin-labeled to allow immobilization on streptavidin metal beads. The in vitro transcription reactions contained immobilized template (100 ng of each template) and nuclear extracts (100 μg) prepared from either wild type (WT) or *cct1-2* yeast grown to log phase, shifted to 37°C for 4 h, and then collected. The cell pellets were used to prepare nuclear extracts as described above. RNA transcripts were detected using standard primer extension reactions and radiolabeled primers designed to detect the upstream (aberrant) or downstream (coding) transcripts.[104]

Template pull-down

To assess TRiC binding to the *DRN1-VAS1* DNA template, 500 μg of nuclear extracts were incubated with 3–4 μg of immobilized template in transcription buffer mix (100mM potassium acetate pH 7.6, 20 mM HEPES pH 7.6, 1 mM EDTA, 5 mM MgOAc, 2 μg creatine phosphokinase, 2 mg phospho creatine, 0.3 mM ATP) to a final volume of 200 μl for 15 min at room temperature. The beads were then washed thrice with transcription buffer mix before boiling in Laemmli buffer for immunoblotting.

Purification of TAP-tagged Proteins and CBP-tagged CCT complexes

TAP-tagged proteins were purified from frozen yeast pellets collected from 3 L of culture. Pellets were ground with dry ice in a coffee grinder and added to 10 ml of E buffer (20 mM HEPES · KOH pH 7.5, 350 mM NaCl, 0.1% Tween 20, 10% glycerol, 1 mM DTT, 1xPI). After clarification at 17,000 rpm for 15 min at 4°C, lysates were incubated with 400 μl of washed IgG Sepharose affinity resin (Cytiva) for 3 h at 4°C. Beads were then collected and washed twice with 10 ml E buffer in Poly-Prep Chromatography Columns (BioRad) and underwent overnight TEV cleavage in 5 ml of E buffer with 5 μl of TEV protease (NEB) at 4°C. For 2-step purifications, the elute was supplemented with $CaCl_2$ to a final concentration of 2 mM and was incubated with 300 μl calmodulin affinity resin (Agilent) for 3 h at 4°C. Calmodulin beads were washed twice before elution with 10 mM EGTA for 5 minutes at room temperature. Both 1-step and 2-step purified proteins were concentrated with 10 kDa Amicon Ultra-4 Centrifugal Filter units (Millipore).

CBP-tagged CCT complexes were purified from strains containing the plasmid encoding CCT6-CBP. Briefly, frozen cell pellets from 3 L of culture were ground with dry ice and recovered using 10 ml buffer A (200 mM NaCl, 50 mM HEPES · KCl pH 7.4, 5 mM CaCl2, 20% glycerol, 1xPI). The lysate was clarified at 17,000 rpm for 30 min at 4°C before incubating with 300 μl of washed calmodulin affinity resin (Agilent) for 3 hours at 4 °C. The beads were then washed with 20 ml buffer A and 20 ml buffer B (500 mM NaCl, 50 mM HEPES · KCl pH 7.4, 2 mM CaCl2, 20% glycerol). The sample was eluted with 2 ml elution buffer (100 mM NaCl, 50 mM HEPES · KCl pH 7.4, 10 mM EDTA pH 8, 10% glycerol, 1xPI) and concentrated.

Microscopy

Live cell microscopy of Cct2-GFP and Cct6-GFP was carried out on a Zeiss LSM900 confocal laser scanning microscope equipped with an Airyscan 2 detection unit.[105] 5 μm z-stacks were collected at intervals of 0.14 μm. Imaging was performed with a 63x/1.4 NA oil immersion objective using Immersol 518-F immersion media (Carl Zeiss) and processed in Fiji. Live cell GFP-nanobody depletion images were acquired with a DeltaVision OMX microscope (GE Healthcare). Imaging was performed with a 100x/1.4 NA oil immersion objective. Z-stack slices (0.5 μM) were captured and image processing was done in Fiji. Colocalization analysis for CCT2/6-GFP Rpb3-mCh strains (± Gal) were done using Fiji. For a selected cell, the FITC and A568-mCh channels were split. The outline of the nucleus is manually defined as a Region of Interest (ROI) using the Rpb3-mCh image (A568-mCh channel). Colocalization between the CCT2/6-GFP and Rpb3-mCh signal within the nuclear ROI specified was determined using the ImageJ plugin Colocalization Threshold. For the NES-GFP-nanobody depletion analysis the outline of the nucleus and the whole cell were manually defined as Regions of Interest (ROIs) using the mCh-ER05 (Pho88 variant) image (A568-mCh channel). These outlines were superimposed on the CCT2/6-GFP images (FITC channel) and the integrated density (IntDen) within these regions was calculated using the ImageJ plugin Measure. The proportion of nuclear signal for each strain at the timepoints 0, 6, 12, and 24 h was measured by dividing the IntDen value of the nuclear region by that of the whole cell region. The mean nuclear signal for the 0 h timepoint was then converted to 100%, with all other values being scaled up accordingly.

Cell viability spot-test

A standard yeast spot-test assay was used to test cell viability by growing cells to mid-log phase, collecting by centrifugation, and resuspending in water to $O.D._{595}$ = 1. Cells were serially diluted in water and spotted (10 μl) on to the described media.

Immunoblot figure generation

All immunoblots were visualized using an Invitrogen iBright CL1000, analyzed using NIH ImageJ, for Figures 1B, 1C, 6E, 7A, and S5A the shown data was cropped from the original image using Microsoft PowerPoint, all other images were cropped using NIH ImageJ, and all final figures were composed in Microsoft PowerPoint.

QUANTIFICATION AND STATISTICAL ANALYSIS

All qRT-PCR and immunoblotting experiments were performed for n ($n \geq 3$) biological replicates. The data points obtained from the n replicates *were* plotted as bar graphs or scatter plots, where the center is the mean of all measured replicates, and the error bars represent the standard error of mean (SEM) of the data set. For each experiment, the exact value of n, as well as the specific details used to create the representative graph h*ave* been detailed in the respective figure legend. Statistical analysis was performed in GraphPad Prism 8.0.2, using unpaired student's t-tests (p-value < 0.05 cutoff) for all quantifications. Statistical significance was calculated using a p-value cutoff of 0.05, and represented as follows: * = $0.01 < p < 0.05$, ** = $0.001 < p < 0.01$ and **** = $p < 0.0001$.